ABSTRACT

Title of Document: DAMAGE DETECTION IN FIBER REINFORCED CONCRETE WITH ULTRASONIC PULSE VELOCITY TESTING

Rongjin Hong, Master of Science, 2012

Directed By: Professor Dimitrios G. Goulias
Department of Civil and Environmental Engineering

In concrete, fatigue and freeze-thaw are associated with the progressive growth of internal microcracks. The Ultrasonic Pulse Velocity (UPV) technique, one of the most widely used Nondestructive Testing (NDT) methods, is promising in evaluating internal microcracks and eventually detecting damage. The primary objective of this research was to determine the effectiveness of using UPV to detect damage development in polypropylene fiber reinforced concrete under fatigue and freeze-thaw conditions. In order to realize this, i) several experiments were conducted on control samples to assess the response and limitations of UPV, and ii) fatigue and freeze-thaw samples were tested with UPV to evaluate its ability to detect crack development. In terms of modeling, three alternative models were examined and presented relating UPV with porosity and damage.

DAMAGE DETECTION IN FIBER REINFORCED CONCRETE WITH ULTRASONIC PULSE VELOCITY TESTING

By

Rongjin Hong

Thesis submitted to the Faculty of the Graduate School of the
University of Maryland, College Park, in partial fulfillment
of the requirements for the degree of
Master of Science
2012

Advisory Committee:
Professor Dimitrios G. Goulias, Chair
Professor M. Sherif Aggour
Professor Amde M. Amde

Dedication

To my dear parents and my heavenly father

Acknowledgements

I would like to acknowledge the following people whose enormous contributions led to the successful completion of this thesis:

I would like to thank my advisor Professor Dimitrios G. Goulias for his continuous guidance, tremendous patience and precious suggestions throughout this entire research. Also thanks for his valuable instructions on my general academic pursuits. Moreover, thank him for his extraordinary tolerance with my poor eloquence.

I would like to thank Professor M. Sherif Aggour for taking time off his busy schedule to serve as a committee member.

I would like to thank Professor Amde M. Amde for graciously lending his time to serve as a committee member.

I would like to thank Ehsan Aramoon, who has offered countless great help in the lab.

I would like to thank Daniel Butler, my good friend in the department, who has provided so much time and so many suggestions in reviewing this thesis.

I gratefully appreciate my girlfriend, Jiena Zhu, for her unyielding support and understanding at the time of pressure.

I would like to thank my brothers and sisters in the church for nonstop praying for me. Even when I didn't hear it, I knew they were praying for my strength.

I would like to express my gratitude to my dear parents, my dear sister and brother, for their family-exclusive encouragement no matter what I face.

Table of Contents

List of Tables

List of Figures

1 Introduction

1.1 Background

In concrete, fatigue is mainly associated with the progressive growth of internal microcracks, which results in a significant increase of irrecoverable strain. At the macro level, this manifests as changes in the material's mechanical properties [1]. Because fibers have the advantage of bridging the microcracks and retarding the crack growth, fiber reinforced concrete (FRC) has been introduced and widely studied.

Freeze-thaw damage is also a reflection of progressive cracking in concrete. Deterioration of concrete as a result of freeze-thaw actions occurs after the concrete is critically saturated, when approximately 91 % of its pores are filled with water. When water freezes, its volume increases by about 9 %. Since there is no space for this volume expansion to take place within the mass of concrete, water freezing will eventually cause cracking. This distress is cumulative and will continue throughout successive cycles over multiple winter seasons, resulting in repeated loss of concrete surface, in the form of scaling. Hence, the use of polypropylene fibers in concrete to transfer stresses is beneficial when the concrete cracks under freeze-thaw effects [2].

Nondestructive Testing (NDT) is an effective tool in evaluating structural integrity and eventually revealing internal microcracks. NDT is implemented without doing harm, stress or destroying the test object. The Ultrasonic Pulse Velocity (UPV) has been used since the early 1940s. In UPV, the transmission of ultrasonic waves over a certain distance is measured with the time of the waves to travel through the material. Frequencies between 25-250 kHz are commonly used since the wavelengths dictate the

ability of UPV to detect crack sizes and to overcome aggregate. The typical wave velocities for concrete range from 3500 m/s to 4500 m/s. The use of such wave measurements for estimating concrete properties, like the dynamic modulus of concrete, represents one of the most common NDT techniques for testing concrete today [3].

1.2 Research Objectives

The primary objective of this investigation was to determine the effectiveness of using UPV to detect damage in fiber reinforced concrete under fatigue and freeze-thaw conditions. With the aim of developing the relationship between UPV and concrete integrity, the following specific objectives were identified:

1. To obtain an accurate interpretation of UPV measurements.

2. To develop a comprehensive understanding of the influences of concrete properties and conditions on UPV.

3. To develop models to relate UPV and concrete porosity.

4. To study the response of UPV in function of different measurement setups using artificially damaged concrete and to find out the best setup for a successful measurement under fatigue testing conditions.

5. To perform laboratory analyses for assessing the capability of UPV to detect concrete damage.

6. To determine the response of UPV in detecting cracking of concrete with fatigue cycles.

7. To determine the response of UPV for detecting cracking within concrete with freeze-thaw cycles.

1.3 Organization of the report

The first chapter presents the introduction, research objectives and the organization of this thesis. Chapter 2 presents an extensive literature review of existing studies on the fatigue and freeze-thaw behavior of concrete, especially FRC, as well as the use of UPV. Chapter 3 presents the material properties and testing plan. In Chapter 4, the UPV method and its relationships to concrete properties and conditions are discussed in detail. Chapter 5 discusses the effectiveness of employing UPV under fatigue test. Chapter 6 addresses the results and modeling related to freeze-thaw effects and UPV. Finally, Chapter 7 presents the conclusions and recommendations.

2 Literature Review

2.1 Introduction

Studies on Ultrasonic pulse velocity (UPV) have established that the characteristics of waves propagating through concrete depend primarily on the elastic properties of the material [4]. With the commercially available equipment, the use of UPV technique is currently very common to determine the concrete quality, monitor service wear, and find potential sever zones in a testing object. In spite of the UPV's success, the heterogeneous properties and complex structure of concrete material, on both microscopic and macroscopic levels, sometimes cause problems in interpreting the behavior of ultrasonic pulses in concrete.

Structures, which are subject to recurrent forces, such as piers resisting sea waves, buildings buffeted by wind action, and pavements under automobile traffic, steadily become pliable, which may eventually lead to fatigue failure of the structures. Although it has been worldly used as a construction material, there is a lack of knowledge regarding the fatigue failure of concrete compared to ferrous materials because of the heterogeneous nature of a concrete mix. This lack of understanding is even more pronounced for fiber-reinforced concrete (FRC).

The effects of freeze-thaw cycles are one of the major durability concerns of concrete. The problem comes from the freezing of water in the cement paste or susceptible aggregates. Since the freezing of water causes it to expand in volume, which may eventually pose an issue to concrete integrity and durability [5]. Although there has been much research on the effects of water freezing on concrete, the mechanisms of freeze-thaw still have some critical questions left unanswered.

The objective of this chapter is to review past research on FRC and its fatigue and freeze-thaw performance, as well as the UPV method and its application especially under fatigue and freeze-thaw conditions.

2.2 Properties of Polypropylene Fiber Reinforced Concrete

2.2.1 Materials and Mixtures of Polypropylene Fiber Reinforced Concrete

Polypropylene fibers are hydrophobic, which do not bond through chemical reaction in the concrete mix, but by mechanical interaction, called pegging. A previous study by Ozyildirim et al. [6] has used 19 mm fibrillated polypropylene fiber, along with 377 kg/m^3 of cementitious material consisting of 60 % Type I/II cement and 40 % ground granulated blast furnace slag (by weight). The coarse aggregate was a granite gneiss with a nominal maximum size of 13 mm and the fine aggregate was siliceous sand. The mix design is shown as shown in Table 2.1. High range water reducing admixture (HRWRA) was added to compensate for the workability.

Similarly, Nagabhushanam et al. [7] tested concrete using the mix design in Table 2.2.

2.2.2 Properties of Fresh Concrete

Satisfactory workability can be maintained by adjusting both HRWRA and w/c ratio [8]. The properties of fresh concrete in Ozyildirim's study [6] is shown in Table 2.3.

Table 2.1 Mixture Design (Source, [6])

Mix	Fiber Content (%)	Coarse Aggregate (kg/m^3)	Fine Aggregate (kg/m^3)	Cement (kg/m^3)	Slag (kg/m^3)	w/c Ratio	HRWRA (ml)	AEA (ml)
SPL	0	890	839	226	151	0.45	0	67
SP1	0.2	890	839	226	151	0.45	1360	67
SP2	0.3	890	839	226	151	0.45	1360	67
SP3	0.5	890	839	226	151	0.45	1360	67
SP4	0.7	890	839	226	151	0.45	1922	67

Note: HRWRA = High Range Water Reducer Admixture, AEA = Air Entrainment Admixture

Table 2.2 Mixture Design (Source, [7])

Mix	Fiber Content (%)	Coarse Aggregate (lbs)	Fine Aggregate (lbs)	Cement (lbs)	w/c Ratio	SPD (ml)	AEA (ml)
NP4	0	187.8	187.8	79.2	0.4	180	25
NF1	0.1	187.8	187.8	79.2	0.4	240	25
NF7	0.1	187.8	187.8	79.2	0.4	240	25
NF3	0.5	187.8	187.8	79.2	0.4	330	25
NF5	0.5	187.8	187.8	79.2	0.4	330	25
NF2	1	187.8	187.8	79.2	0.4	380	25
NF1	1	187.8	187.8	79.2	0.4	550	30

Note: SPD = Superplasticizer Dosage, AEA = Air Entrainment Admixture

Table 2.3 Properties of Fresh Concrete (Source, [6])

Fiber	Fiber Content (kg/m^3)	Fiber Content Vol%	Slump (mm)	Inverted Slump (s)	Air (%)	Unit Weight (kg/m^3)
Polypropylene Fibrillated	1.8	0.2	30	5	5.3	2340
	2.7	0.3	25	4	6.3	2280
	4.6	0.5	15	10	5.7	2280
	6.4	0.7	15	6	7.5	2250

2.2.3 Compressive and Flexural Strength of Polypropylene Fiber Reinforced Concrete

Compressive strength of concrete mixes is determined according to ASTM C39 using concrete cylinders while flexural strength (Modulus of Rupture; Mr) is evaluated by applying third point loading according to ASTM C78 with concrete beams. The results in the study by Nagabhushanam et al. [7] are shown in Table 2.4.

Table 2.4 Hardened Concrete Properties (Source, [7])

Mix	Fiber Content (Kg/m^3)	(Vol%)	Compressive Strength (MPa)	Mr (kPa)
NP4	0	0	40.7	5.44
NF1	0.9	0.1	40.9	4.55
NF7	0.9	0.1	46.3	6.13
NF3	4.6	0.5	48	5.82
NF5	4.6	0.5	46.7	5.58
NF2	8.9	1	44.2	5.2
NF1	8.9	1	38.4	4.82

As shown in Table 2.4, the compressive strength increased slightly with fiber content to some extent and flexural strength increased with fiber content until 0.1 % and decreased as more fibers were added.

On the other hand, some other research [9] has indicated that compressive strength deceases with the increase of fiber volumes instead.

Bayasi et al. [10] concluded that various factors can affect the behavior of FRC, which include fiber length, aspect ratio, the volume fraction of fiber, fiber orientation, fiber shape, fiber bond characteristics, etc.

2.3 Fatigue Behavior of Polypropylene Fiber Reinforced Concrete

2.3.1 Fatigue Strength of Polypropylene Fiber Reinforced Concrete

Fatigue strength is the maximum flexural fatigue stress at which a beam can withstand two million cycles of fatigue loading. The endurance limit is the fatigue strength expressed as a percentage of the flexural strength of plain concrete.

According to ACI [11], applications in slab-on-grade which have collated fibrillated polypropylene fiber, with a content up to 0.3 % by volume, can show a dramatic increase in the fatigue strength, by 15 to 18 % compared to plain concrete.

2.3.2 Fatigue Life and Modeling

The fatigue behavior and resistance of FRC have been studied extensively. Most of the researchers adopted a relationship between stress level, S, the ratio of the maximum loading stress to the modulus of rupture, σ_{max}/Mr, and the number of loading cycles, N. This relationship is known as the Wholer equation, as illustrated in Equation 2.1. Another form of the relationship incorporates the stress ratio R, the ratio of the minimum to the maximum stress. This modification is shown as Equation 2.2.

$$\boldsymbol{S = \frac{\sigma_{max}}{Mr} = a - bLog(N)} \qquad (\mathbf{2.1})$$

$$\boldsymbol{S = \frac{\sigma_{max}}{Mr} = 1 - b(1-R)Log(N)} \qquad (\mathbf{2.2a})$$

$$\boldsymbol{R = \frac{\sigma_{min}}{\sigma_{max}}} \qquad (\mathbf{2.2b})$$

where *a* and *b* are experimental coefficients.

In the study by Lee [1], it was stated that the majority of researchers have found the addition of fibers beneficial to the fatigue performance of concrete, to some extent. However, it was also indicated that the quantitative nature of this benefit is difficult to determine, since parameters related to loading conditions, such as load frequency, boundary conditions etc, will all impact FRC's fatigue performance.

2.4 Freeze-Thaw Behavior of Concrete

2.4.1 Freeze-Thaw Theories and Effects

It is generally accepted that there are three major hypotheses explaining the effects of freeze-thaw: hydraulic pressure theory, osmotic pressure theory and desorption theory.

The general scenario is described as follows: the ice formed from water would expand by approximately 8 ~ 9 % in volume, which leads to the movement of the ice and pushes the liquid water ahead of it. When such flows of water is restrained by the limitations of pore space, expansive hydraulic pressures build up, the development of which eventually brings in microcracking, or an enlarged porosity [5]. Moreover, the expelled water from capillaries absorbs more solutes driven from the frozen pure water, which produces a concentration gradient and causes osmotic pressure [5]. Finally, the desorption theory proposes that water in aggregate pores can be forced out due to the differentials of vapor pressure [12].

According to the hydraulic pressure theory, when the flow path exceeds a critical length, the pressure will exceed the paste strength. The saturation level at this turning

point is defined as “critical saturation”, which was first calculated to be 91.7 % saturation [13] and later found to be lower [14].

2.4.2 Freeze-Thaw Test

Concrete beams are tested for resistance to freeze-thaw by applying the rapid freezing and thawing test according to ASTM C666. Deterioration of specimens is determined by the resonant frequency method, at intervals not exceeding 36 cycles of exposure.

While this is the most widely used test method, it was criticized for the variability of the results both within and between laboratories [15].

2.4.3 Effects of Polypropylene Fibers on Freeze-Thaw

Most researchers have reported the benefits of freeze-thaw resistance of polypropylene FRC. For example, Bayasi et al. [16] indicated some benefits of fibers on scaling prevention. Al-Tayyib et al. [17] found an improved surface performance of FRC, which can effectively retard the deterioration process of the surface skin. On the other hand, ACI [11] pointed out the fiber additions have no significant effects on freeze-thaw resistance of concrete.

2.5 Ultrasonic Pulse Velocity Method

2.5.1 Theory of Pulse Propagation through Concrete

When an impulse is applied to a solid material, a disturbance is caused to travel through the solid mass as stress waves, or mechanical waves, consisting primarily of three modes. Surface, or Rayleigh, waves, which have an elliptical particle displacement, are the slowest. Shear, or S waves, with particle displacement perpendicular to the direction of travel, are faster. The third type, longitudinal, also called P waves, with particle displacement in the direction of travel, are the fastest and the most important [18]. The characteristics and particle motions are illustrated in Figure 2.1.

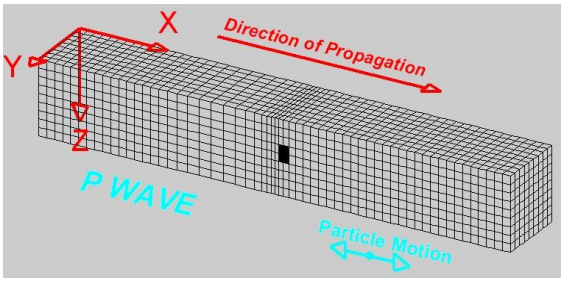

a) P waves

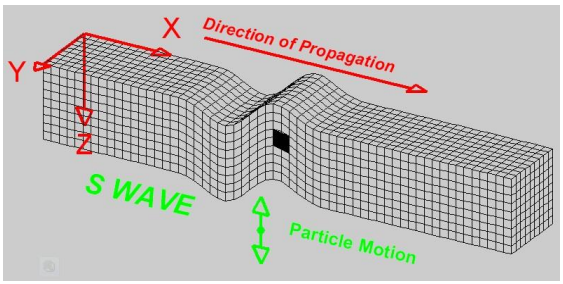

b) S waves

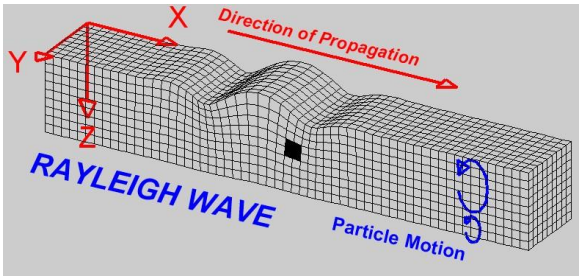

c) Rayleigh waves

Figure 2.1 Characteristics and Particle Motions of the Three Waves

2.5.2 Speed of Waves and Dynamic Modulus of Concrete

In an infinite, homogeneous, isotropic elastic medium, the P wave speed is given by:

$$\boldsymbol{C_p = \sqrt{\frac{(1-\nu)}{(1+\nu)(1-2\nu)} * \frac{E_d}{\rho}}} \qquad (\mathbf{2.3})$$

where:

V = compression wave velocity, km/s

Ed = dynamic modulus of elasticity, kN/mm^2

ρ = density, kg/m^3, and

ν = dynamic Poisson's ratio.

In bounded materials, if the lateral dimension of the material is much less than the wavelength(s), the wave speed is relatively constant, independent of the dynamic Poisson's ratio, and hence, the dynamic modulus of elasticity is equal to:

$$\boldsymbol{E_d = \frac{C_p^2 \rho}{K}} \qquad (\mathbf{2.4a})$$

$$\boldsymbol{K = \frac{(1-\nu)}{(1+\nu)(1-2\nu)}} \qquad (\mathbf{2.4b})$$

2.5.3 Ultrasonic Pulse Velocity Test

In practice, pulse velocity through concrete is measured by applying the standard test according to ASTM C597 and calculated with Equation 2.5.

$$\boldsymbol{V = \frac{L}{t}} \qquad (\mathbf{2.5})$$

where:

V = ultrasonic pulse velocity, m/s,

L = distance between centers of transducer faces, m, and

t = wave transit time, s.

As concrete is a highly heterogeneous composite material, the propagation of waves cannot be smooth, resulting in a variation between the measured path and the propagated path. Furthermore, stress waves are subject to attenuation, reflection and refraction at the interface of different materials, analogous to the light rays [19]. Therefore, the measured UPV shows, in most cases, variations from the wave speed.

2.5.4 Test Equipment and Transducer Arrangement

In measuring UPV, the equipment generates a pulse, transmits this pulse to the material, receives and amplifies the pulse. The basic circuitry and a commonly used instrument are shown in Figure 2.2.

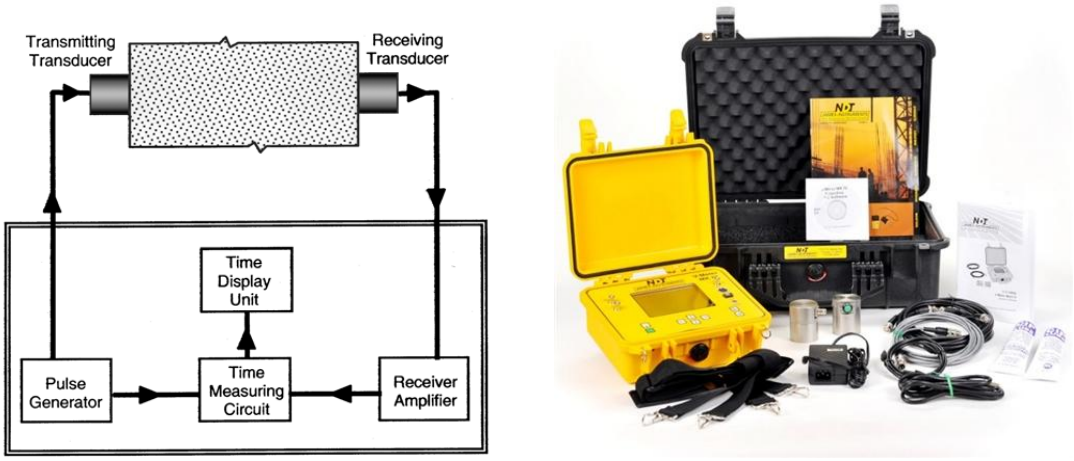

a) Schematic of UPV Apparatus (Source of ASTM C597)

b) A commonly used UPV instrument (Source of James Instruments, Inc.)

Figure 2.2 UPV Test Equipment

There are three basic ways that the transducers may be arranged, as shown in Figure 2.3. These are: i) opposite faces (direct arrangement); ii) adjacent faces (semi-direct arrangement); and iii) same face (indirect arrangement).

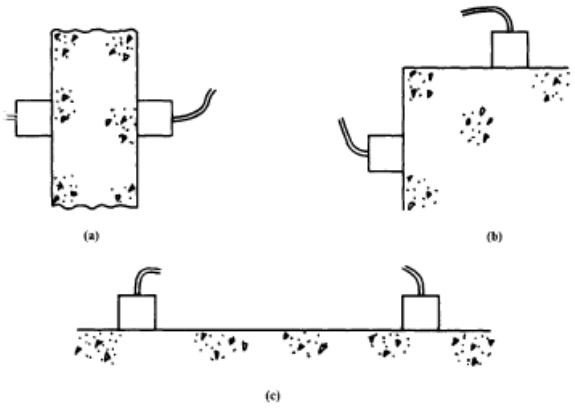

a) Direct, b) Semi-Direct, c) Indirect
Figure 2.3 Transducer Arrangement
(Source of James Instruments, Inc.)

The direct arrangement is the most desirable and the most satisfactory, since maximum energy of the pulse is transmitted and received with this arrangement. The semi-direct arrangement can be used when the transducers are not too far apart. The third arrangement, indirect, is the least satisfactory because the amplitude of the received signal is quite low, and thus is used when only one surface of specimen can be tested. No matter which arrangement is chosen, couplant such as petroleum jelly should be used to avoid air pockets between specimen and transducer, which may introduce errors in the indicated transit time.

2.6 Factors Affecting Ultrasonic Pulse Velocity

2.6.1 Ultrasonic Pulse Velocity and Temperature

Temperature can affect UPV and the corrections are shown in Table 2.5.

Table 2.5 Corrections for UPV Due to Temperature Changes (Source, [19])

Concrete Temperature (± ℃)	Corrections (%)	
	Air-Dried Concrete	Water-Saturated Concrete
60	5	4
40	2	1.7
20	0	0
0	–0.5	–1
Under -4	–1.5	–7.5

2.6.2 Ultrasonic Pulse Velocity and Water Content

Ye et al. [20] studied the microstructure development of concretes and concluded that lower w/c mixes have higher UPV, due to higher amount of total and connected solids. Trtnik [21] stated that the w/c does not play a very significant role on the UPV-strength relationship, whereas Madandoust et al. [22] found that the w/c affects this relationship at later ages of hydration.

On the other hand, the water present in the pores of concrete during testing has accelerating effects on UPV, since ultrasonic waves propagate faster in water than in air. For example, ASTM C597 indicates UPV in saturated concrete may be up to 5 % higher than in dry concrete. Ohdaira [23] reported that UPV is proportionate to the water content in concrete and can be used for assessing the changes in concrete strength. This was confirmed by Yaman [24], who later explained the difference between saturated and dry

states are caused by the changes in pore shape/connectivity when the moisture is added to or removed from the capillary pores.

It was recently recognized that the distribution of water within concrete can also affect UPV [25].

2.6.3 Ultrasonic Pulse Velocity and Porosity

According to Popovics [26], modulus is assumed to be in a power law relation to the porosity, as

$$\boldsymbol{E = E_0(1 - p)^c} \qquad (\mathbf{2.6})$$

where *c* is an empirical fitting parameter and E_0 is the modulus of the material at zero porosity. As density is related to porosity by

$$\boldsymbol{\rho = \rho_0(1 - p)} \qquad (\mathbf{2.7})$$

Then insertions of Equations 2.6 and 2.7 into Equation 2.4 yields

$$\boldsymbol{V = V_0(1 - p)^a} \qquad (\mathbf{2.8})$$

where V_0 is ultrasonic pulse velocity at theoretical zero porosity and $a = (c-1)/2$.

Lin et al. [27] confirmed that UPV increases with a decreasing w/c due to decreasing porosity. Ohdaira et al. [23] developed a linear relationship between the amount of water in saturated samples, representing porosity, and UPV.

As a matter of fact, four categories of pores are present in concrete [28]: gel pores, capillary pores, entrained air voids and entrapped air voids. Among these four, capillary pores, with a size of 10 nm to 10 μm, may be empty, partly filled, or completely saturated by 40 days. Entrained air voids are on the order of 100 μm and entrapped air voids on a scale of 1 mm to 1 cm. Yaman et al. [24, 29] classified these pores into active (capillary

with some gel) pores and non-active (entrained air) pores, the former of which influence concrete properties more significantly with a decreasing trend. They developed the relationships between UPV and porosity and found that some capillary pores are opened and filled with water under saturation.

2.6.4 Ultrasonic Pulse Velocity and Cement Hydration/Concrete Hardening

Researchers [30-32] have found that there are three stages of UPV evolution after mixing. During Stage I, the concrete is a water-like viscous cement suspension, and the air bubbles present in the concrete determine an initial UPV of about 1300m/s. Stage II exhibits an obvious increase of UPV because more hydration products fill in the pores and change the propagation path to be like along solid. Finally, Stages III starts when the pores are filled up by the hydration products.

In terms of hardened concrete, Khan et al. [33] and Popovics et al. [34] confirmed that UPV increases with age with a decreasing rate and that UPV through concrete increases faster than that through mortar. The trend is shown in Figure 2.4.

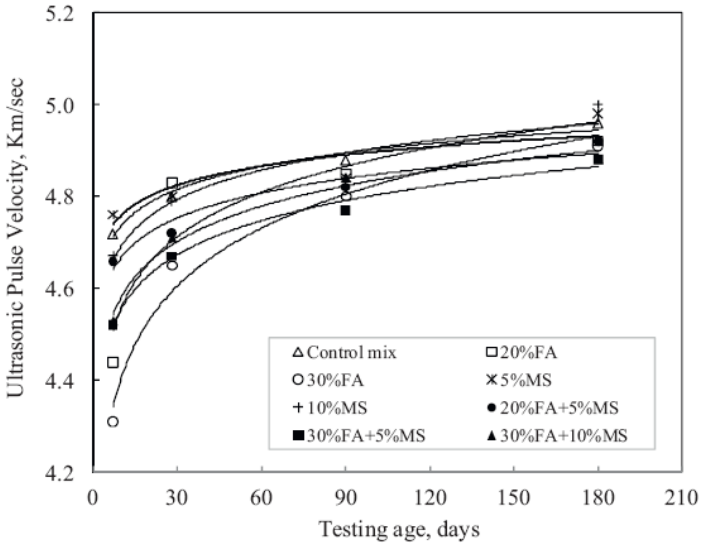

Figure 2.4 UPV of Concrete Containing Cementitious Composites with Age (Source, [33])

2.6.5 Ultrasonic Pulse Velocity and Density

Density of concrete is related to the porosity and solid fraction, as already shown in Section 2.6.3. Thus higher-density samples should have a higher UPV. Popovics et al. [34] confirmed this relationship, regardless of the compositions of specimens. Panzera et al. [35] have proposed a linear relationship between UPV and bulk density.

2.6.6 Ultrasonic Pulse Velocity and Compressive Strength

A variety of correlation equations between the strength and UPV of concrete have been proposed and examined. They are listed in Table 2.6.

Table 2.6 Relationship between Compressive Strength, fc, and Pulse Velocity, V

Equation	R^2	Reference
$fc = 0.0854 \exp(1.2882V)$	0.64	[21]
$V = 1.92fc^{0.20}$	0.82	[33]
$fc = 1.146 \exp(0.77\ V)$	0.80	[36]
$fc = 1.19 \exp(0.715\ V)$	0.59	[37]
$fc = 8.4 \times 10^{-9}(V \times 10^3)^{2.5921}$	0.42	[38][a]
$fc = 1.2 \times 10^{-5}(V \times 10^3)^{1.7447}$	0.41	[38][b]
$fc = \exp[(-3.3 \pm 1.8) + (0.0014 \pm 0.0004)(V \times 10^3)$	0.48	[39]
$fc = 15.533UPV - 34.358$	0.92	[40]

a: For wet concrete. b: For dry concrete.

However, it is generally accepted [13, 34] that for a specific mix design, an UPV-compressive strength calibration curve should first be established based on the mix before the relationship can be used.

2.6.7 Ultrasonic Pulse Velocity and Crack Growth

Hauwaert et al. [41] studied the relationship between UPV, peak amplitude, energy and the crack length during crack growth concrete. The 150 x 150 x 150 mm^3 cubes were progressively cut in steps of 10 mm and UPV were measured.

They discovered that transit time would be affected only after the saw-cut exceeds the "track", the portion enclosed between the two extreme lines connecting the transducers, as in Figure 2.5. After the cut was larger than the track, the arrival time and the saw-cut length could be related linearly.

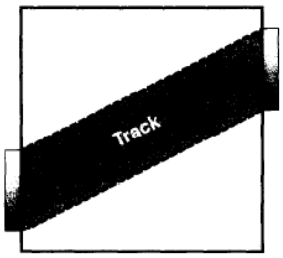

Figure 2.5 Definition of a "Track" between Transducers (Source, [41])

2.6.8 Ultrasonic Pulse Velocity and Freeze-Thaw Effects

As cited by Nixon [42], Malhotra started to utilize UPV technique in 1976 to assess the freeze-thaw resistance of concrete with recycled aggregates. The results showed that UPV decreased after a certain number of freeze-thaw cycles, some of which as high as 4 %, after more than 600 cycles. Several other researchers have also employed UPV as a tool in freeze-thaw testing. Richardson et al. [43] found that freeze-thaw damage can be reflected by a reduction in UPV. In another study by Richardson et al. [2], a significant decrease in UPV was discovered on the plain concrete after 150 freeze-thaw cycles. Also, enhanced durability of polypropylene FRC was observed. Kelly et al. [44] discovered that the mixes worst affected by scaling had the largest increases in transit time. Şahmaran et al. [45] reported that the changes in UPV of ECC matrix specimens was -30.9 %, in accordance with a -7.3 % mass change, after 210 freeze-thaw cycles. Héctor et al. [46] discovered that under thawing conditions, the progressive deterioration of concrete leads to a UPV decrease, while under freezing conditions the ice in the microcracks results in an increase.

Other researchers have found some limitations of UPV. In a study by Erdélyi et al. [47], UPV was found to significantly decrease after freeze-thaw cycles only in oven dried

specimens, but not on NaCl-saturated samples. Selleck et al. [48] reported that UPV was insensitive to changes caused by microcracking.

2.7 Conclusion

In this chapter, previous studies on polypropylene fiber reinforced concrete and its performance under fatigue and freeze-thaw conditions were analyzed and results from UPV testing were summarized. Although much has been studied about polypropylene fiber reinforced concrete, including its performance under both fatigue and freeze-thaw conditions, there are still a manifold of questions to answer regarding the cracking mechanism. Indices characteristic of crack size, shape and location etc. have to be represented. Meanwhile, the UPV method, as one of the most widely used NDT techniques in revealing changes of concrete properties, shows promise in providing these indices. However, the reality is that it has been used most likely as a supplementary test, due to the limited information provided by this method.

When studying UPV, water content, porosity, density are related critical parameters. While the relationships between porosity and saturated UPV as well as dry UPV have been studied, no effort was taken to quantify the status of partial saturation. While the relationships between UPV and w/c ratio as well as the water present in the pores after hydration have been studied, no effort was taken to unify the influence of these two “kinds” of water. The solution to these key questions is believed to create a broader vision to apply UPV to discover more information underneath and detect cracking.

3 Materials and Testing Plan

3.1 Materials and Mix Design

The concrete was made under MD 7 requirements. The materials used consisted of Skarete® Type I-II Portland cement, natural sand as the fine aggregate and #57 stone as coarse aggregate. THE FIBER DEPOT™, 19 mm long fibrillated polypropylene fiber, was used. A Sika® air-entraining admixture and a Sika® high range water-reducing admixture were used to maintain workability at the designated water cement ratio (w/c) of 0.44. The synergistic effects of these admixtures produced concretes using 0.8 % reinforced fibers with enhanced finishing strength.

The mix design is presented in Table 3.1.

The cylinders used had a dimension of 101.6 x 203.2 mm (4 x 8 inch) and the beams used had a dimension of 76.2 x 76.2 x 304.8 mm (3 x 3 x 12 inch).

Table 3.1 Materials in $1m^3$ of Concrete

Materials	Stone #57	Sand	Cement	Water	Fiber	Air Entrainer	Water Reducer
Weight (kg)	2747.4	1876.0	1245.0	547.8	20.7	0.8	3.1

3.2 Use of Nondestructive Testing Device

Two Nondestructive Testing (NDT) devices based on Ultrasonic Pulse Velocity (UPV), Model V-C-9900 with a frequency of 54 kHz and Model C-4902 with 36 kHz, were used. Since wavelength is inversely proportional to the frequency, V-C-9900 has a

shorter wavelength and thus is supposed to be more sensitive and attenuation-susceptible. Comparisons of the two wavelengths were conducted in different occasions through this study.

3.3 Testing Plan

In order to determine the effectiveness of using UPV to detect damage in fiber reinforced concrete under fatigue and freeze-thaw conditions, the following specific tests were targeted:

1. Inverted slump was measured on fresh concrete and air content was performed to measure the amount of air-entrainment.

2. Compressive and flexural strength were measured on hardened concrete.

3. Repeated pulse velocity tests were taken to assess the repeatability of the device and the reproducibility of UPV measurements under different conditions.

4. Various pulse velocity tests were conducted to investigate the influences of concrete properties and environmental conditions on UPV.

5. Comparisons of wave frequencies and testing setups were considered to examine the response of UPV with fiber reinforced concrete (FRC).

6. Fatigue test was conducted to study the ability of UPV in detecting damage under fatigue.

7. Freeze-thaw testing was conducted to assess the ability of UPV to detect cracking under freeze-thaw conditions.

The raw data collected in different phases of this research were examined using a statistically based procedure, which is used by SHA and included in MSMT734. This

procedure is based on a two-tailed t-test with a level of significance of 1 %. The use of a two-tailed test means that the outlier may be either on the high or the low side of the average. The 1 % level of significance means that if it is decided that the value is an outlier, there is only a 1 % chance that it is not.

4 Concrete Properties and the Relationships with Ultrasonic Pulse Velocity

4.1 Fresh Concrete

Four batches of concrete were made in this study. Air content and inverted slump were measured according to ASTM C231 and ASTM C995, respectively. The results for each batch are shown as follows.

Table 4.1 Fresh Concrete Properties

Batch	Air Content (%)	Inverted slump (s)
1	5.5	10
2	6.1	12.8
3	6.2	9.5
4	--	9

An outlier analysis method (as described in section 3.3) was used in these data. It can be seen that the air content and inverted slump are consistent among the four batches. The average air content is 5.9 % while the average inverted slump is 10.3 seconds.

4.2 Compressive Strength

Compressive strength, *fc*, was conducted, according to ASTM C39, on cylinders at 4 and 8 weeks from casting. The results, as well as the mean and coefficient of variation (COV), are shown in Table 4.2.

Table 4.2 Compressive Strength of Cylinders

Batch	Age (Days)	Sample	Diameter (mm)	Max Load (kN)	Compressive Strength (kPa)	Mean (kPa)	COV (%)
4	28	1	101.689	269.749	33214	33113	0.7
		2	102.339	273.692	33273		
		3	102.946	273.459	32854		
1	56	1	101.727	297.408	36592	33725	9.3
		2	102.235	249.323	30372		
		3	101.981	279.437	34210		

An outlier analysis (as described in section 3.3) was employed in these data before running the analysis. The samples of 28 days have an average compressive strength of 33,113 kPa while those of 56 days have 33,725 kPa. The difference is 1.8 %, showing a consistency from Batch 1 to Batch 4. Besides, Batch 1 seems to have a higher variability within the samples.

4.3 Flexural Strength

Static flexural strength, *Mr*, was evaluated according to ASTM C78, on beams at 4, 6 and 11 weeks from casting. The results are shown in Table 4.3 and plotted in Figure 4.1.

Table 4.3 Flexural Strength of Beams

Batch	Age (days)	Sample	Depth (mm)	Width (mm)	Max Load (kN)	Flex. Strength (kPa)	Mean (kPa)	COV (%)
4	28	1	77.800	76.937	9.010	4423	4662	5.5
		2	76.954	79.527	10.161	4932		
		3	76.446	77.648	9.192	4631		
1	58	1	76.606	75.421	9.872	5099	4975	9.6
		2	76.556	74.160	10.224	5378		
		3	76.352	77.953	10.832	5449		
		4	76.632	74.930	9.871	5128		
		5	76.810	74.955	8.785	4541		
		6	76.784	74.439	8.165	4253		
	75	1	77.038	79.197	10.750	5228	5035	6.0
		2	76.479	77.546	10.297	5190		
		3	76.606	76.352	9.189	4688		

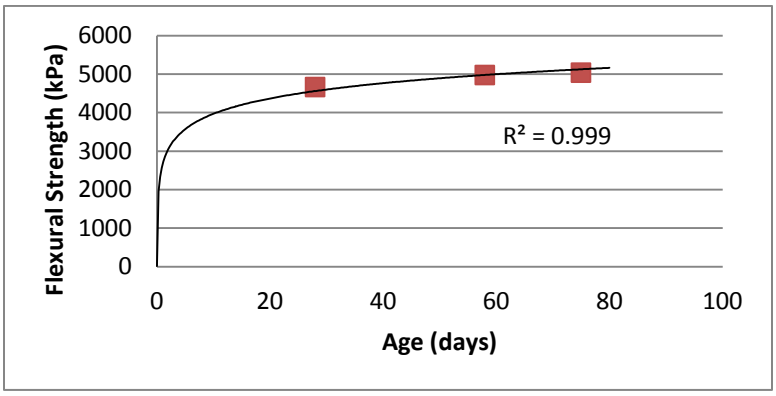

Figure 4.1 Relationship between Flexural Strength and Age

An outlier analysis method (as described in section 3.3) was used in these data and no outlier was found. The average 28-day flexural strength is 4,662 kPa while the average 58- and 75-day flexural strengths are 4,975 kPa and 5,035 kPa, respectively. The flexural strength increases with age, regardless of batch, indicating consistency among batches. On the other hand, a considerable variability exists within each batch. Care should be exercised in analyzing these data.

4.4 Ultrasonic Pulse Velocity and Relationships with Other Factors

4.4.1 Repeatability and Reproducibility of Ultrasonic Pulse Velocity

Ultrasonic Pulse Velocity (UPV) was measured and calculated according to ASTM C597.

Repeated executions of this test on the same material do not always yield numerically identical results. Instead, minor differences exist between tests even if the test is carried out continuously on the same specimen. This is caused by the repeatability error of the Nondestructive Testing (NDT) device. Besides, as presented in Section 2.6, when UPV is measured at a different time, it may result in more varied readings. This randomness of transit time, or UPV, is caused by factors including concrete maturity, temperature, moisture, segregation, transducer arrangement or adherence of transducers to concrete surface etc, and is denoted as reproducibility error. The following testing and analysis were to quantify these errors.

Repeated tests on Sample 5 from Batch 1 were conducted at the four corners of the sample, on three days. When transit time at a specific corner was measured, the transducers were placed attached to the two sides, in a direct method so the length of the beam would be the path length, as shown in Figure 4.2. Corners 1 and 2 are the bottom of concrete during casting while Corners 3 and 4 are the top. After one corner was measured, the concrete beam was turned for another corner to be measured. The transit time readings, and the mean and COV, are shown in Table 4.4.

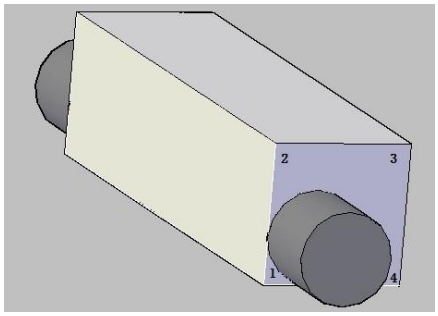

Figure 4.2 UPV Measurement (Measured at Corner 1)

Table 4.4 Repeated Transit Time Readings of Sample 5, Batch 1

Age (days)	61				67				75			
Corner	1	2	3	4	1	2	3	4	1	2	3	4
Transit Time Readings (µs)	65.2	67.1	68.9	69.4	65.4	65.7	67.5	69.1	65.1	64.6	67.2	68.4
	66.2	67.4	70.0	68.8	66.2	66.5	68.6	68.5	65.6	64.5	67.9	68.7
	67.4	68.4	69.4	68.7	66.1	65.7	68.2	68.2	65.2	65.3	67.0	68.4
	66.6	67.4	69.2	69.3	65.7	65.8	67.1	68.4	65.9	64.7	67.5	68.6
	68.2	67.1	68.9	69.2	66.9	66.0	67.0	67.3	65.9	65.2	67.2	68.7
Mean (µs)	66.7	67.5	69.3	69.1	66.1	65.9	67.7	68.3	65.5	64.9	67.4	68.6
COV (%)	1.72	0.79	0.66	0.45	0.86	0.51	1.03	0.95	0.58	0.56	0.52	0.22
Mean of Two Corners (µs)	67.10		69.18		66.00		67.99		65.20		67.96	
Mean of Four Corners (µs)	68.14				67.00				66.58			

Note: Corners 1, 2 are the bottom during casting. Corners 3, 4 are the top during casting.

The outlier analysis method as described in section 3.3 was used in these data before running the analysis. The variability at each corner indicates the repeatability error due to the NDT device. All of the COVs are below 1 % except two cases. With such consistent performance, it was determined that five repeated readings were to be used through this study.

On the other hand, COV in the readings on three different days are 0.89 %, 1.99 %, 1.51 % and 0.58 %, for Corners 1, 2, 3, 4 respectively. The average

measurements are 68.14 μs, 67.00 μs and 66.58 μs with a COV of 1.20 %, indicating the variability among testing days. Moreover, it is seen that Corners 1 and 2 tended to yield lower transit time. Since Corners 1 and 2 are the bottom of concrete during casting while Corners 3 and 4 are the top, the difference in transit time showed the potential of concrete segregation. Therefore, analysis of variance, ANOVA, was used to shed light on the effects of "age" and "corner". The ANOVA is a comparison of all 60 transit time readings listed in Table 4.4. The following hypotheses were used:

H_0: $t_1=t_2=\ldots=t_{60}$;

H_1: transit time is different at different conditions

in which t_1, t_2,…, t_{60} are each of the transit time readings on a specific day at a specific corner. The null hypothesis indicates that neither "age" nor "corner" makes a difference in transit time. The level of significance, $\sigma=0.05$. The distribution for the null hypothesis is presented in Figure 4.3. The Excel built-in tool "ANOVA Two Factor With Replication" was used and the results are presented in Table 4.5.

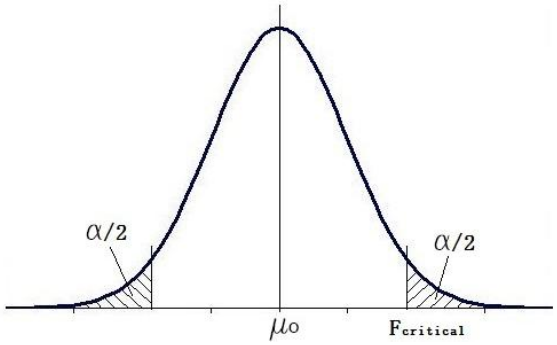

Figure 4.3 Distributions for the Null Hypothesis

Table 4.5 ANOVA: Effects of Age and Corner on Transit Time

Source of Variation	*SS*	*df*	*MS*	*F*	*P-value*	*F crit*
Age	26.11233	2	13.05617	42.65559	2.25E-11	3.190727
Corner	79.9365	3	26.6455	87.05309	1.99E-19	2.798061
Age*Corner	6.881	6	1.146833	3.746801	0.003883	2.294601
Within	14.692	48	0.306083			
Total	127.6218	59				

In Table 4.5, the first row shows the significance of the factor "age". Since F-value is 42.65559, much larger than the critical value F-critical equal to 3.190727. Thus, the null hypothesis was rejected and the factor "age" is significant. The same is valid for the factor "corner", shown in the second row. Since the F-value is 87.05309, much larger than the F-critical equal to 2.798061, the null hypothesis was rejected and the factor "corner" is significant. In addition, there is potential interaction between the two factors, as the third row shows. The fourth row "within" shows the variability in five readings. Therefore, it is crucial to keep consistency regarding which corner to be used as well as to take the concrete age into account.

4.4.2 Effects of Water on Ultrasonic Pulse Velocity

One of the major parameters influencing UPV is moisture residing in different pores. In order to investigate the influence of moisture, ASTM C642 was conducted with minor modifications: Transit time was measured, with transducers placed at the center of cross sections, on samples in SSD condition, and on samples placed into an oven at 75 ℃ to remove part or all of the moisture. The reason this temperature was chosen instead of using the standard (100 to 110 ℃) was to avoid melting of polypropylene fibers or any microcracking due to heating. After removing each sample from the oven, it was cooled

at dry air to room temperature before transit time, weight and length were determined. These steps were repeated until the moisture was removed as much as possible at 75 ℃, meaning there was no difference between two consecutive weight measurements. The cumulative drying time was over 50 hours and the whole process took approximately three to four days.

Absorption α (%) was obtained using Equation 4.1 based on their weight at the completion of the drying.

$$\boldsymbol{\alpha = \frac{W - W_{dry}}{W_{dry}} * 100\%} \qquad (\mathbf{4.1})$$

where:

W = weight in air at the time of measurement, g

W_{dry} = weight in air of oven dry sample, g

The propagation path was determined with the mean of length measurements at four corners, and the transit time was the mean of five transit time readings. UPV was calculated from Equation 2.5. The results are shown in Table 4.6 for Samples M1 through M6 of Batch 4.

Table 4.6 Absorption and UPV (Batch4)

Sample	W (g)	α (%)	UPV (m/s)*
M1	4059.9	2.58 (SSD)	4669
	4050.5	2.34	4679
	4010.1	1.32	4531
	3974.9	0.43	4532
	3958.4	0.02	4485
	3957.7	(Dry)	4432
M2	3809.8	3.01 (SSD)	4440
	3799.9	2.74	4479
	3746.1	1.28	4316
	3698.7	0.003	4305
	3698.6	(Dry)	4300
M3	3967.8	3.17 (SSD)	4493
	3953.1	2.79	4435
	3896.4	1.32	4309
	3848.2	0.07	4253
	3845.7	(Dry)	4234
M4	4011.7	2.74 (SSD)	4694
	3993.3	2.27	4522
	3964.2	1.52	4523
	3954.8	1.28	4424
	3934	0.75	4487
	3916.5	0.30	4361
	3904.7	(Dry)	4363
M5	3942.9	2.89 (SSD)	4537
	3921.0	2.32	4533
	3890.5	1.52	4429
	3881.9	1.30	4431
	3861.6	0.77	4418
	3843.7	0.30	4372
	3832.2	(Dry)	4326
M6	4023.7	2.68 (SSD)	4724
	4016.5	2.50	4679
	4004.0	2.18	4675
	3976.4	1.48	4617
	3946.8	0.72	4535
	3930.1	0.30	4462
	3918.5	(Dry)	4417

* Number of repeated UPV measurements =5

An outlier analysis method (as described in section 3.3) was used in these samples' initial properties, and no outlier was found. The results indicate that each sample shows a proportional decreasing trend with the decrease of absorption or moisture, in accordance with previous studies [23-25, 49]. Although different models have been proposed [23, 49], a linear relationship was used in this study. For example, regression of M1 and M5 yields the following equations, as shown in Figure 4.4.

$$\boldsymbol{V(M1) = 82.3\,\alpha + 4463, with\ R^2 = 0.9042} \qquad \boldsymbol{(4.2a)}$$

$$\boldsymbol{V(M5) = 72.0\,\alpha + 4342, with\ R^2 = 0.9426} \qquad \boldsymbol{(4.2b)}$$

where V is the pulse velocity (m/s) and α is absorption (%).

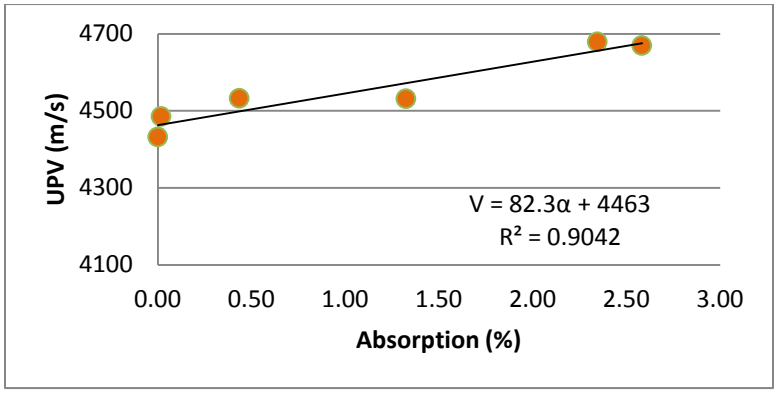

a) Data for Sample M1

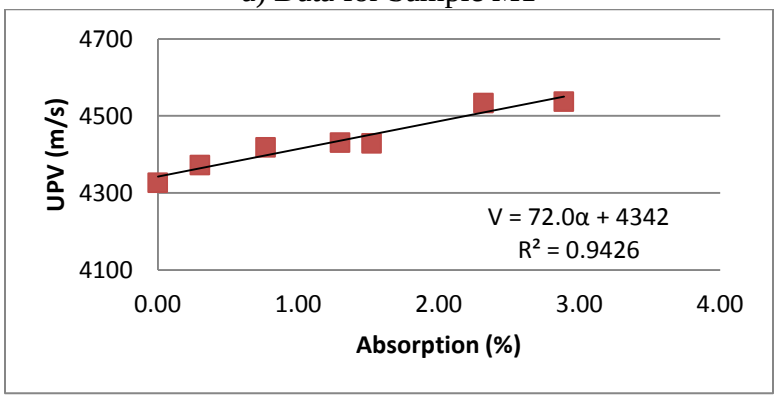

b) Data for Sample M5

Figure 4.4 Relationship between UPV and Absorption (Specific Sample)

In order to derive a general relationship between absorption and UPV, six absorption levels, 0 %, 0.5 %, 1.0 %, 1.5 %, 2.0 %, 2.5 %, 3.0 %, were chosen. At each specific absorption, UPV values were calculated from each sample's regression line and the resulted values were averaged to represent the overall UPV value for that absorption. The results were shown in Table 4.7 and plotted in Figure 4.5, and the obtained relationship is presented in Equation 4.2c.

$$\boldsymbol{V(all) = 82.6\alpha + 4353, with\ R^2 = 1} \qquad \boldsymbol{(4.2c)}$$

where V is the pulse velocity (m/s) and α is absorption (%).

Table 4.7 Absorption and Average UPV

α (%)	UPV (m/s)
0.0	4353
0.5	4394
1.0	4435
1.5	4477
2.0	4518
2.5	4559
3.0	4600

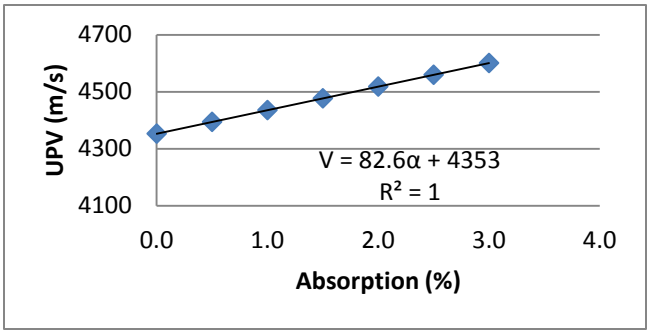

Figure 4.5 Relationship between UPV and Absorption (General)

The reasons for the variability in UPV values among the samples were the objective of the following analysis.

4.4.3 Effects of Porosity on Ultrasonic Pulse Velocity

As mentioned in the Section 2.6.3, there are four different types of pores in the structure of concrete [28]: gel pores, capillary pores, entrained air voids and entrapped air voids. Each one plays a different role on concrete properties and UPV.

While UPV values can be found in Table 4.6, porosity needs to be defined and calculated. In this study, it is defined as the "volume of permeable pore space (voids) in percentage". In order to obtain the volume of the permeable pores and the concrete, the samples were weighed in SSD condition in air and under water, as well as in dry condition in air. (The details of drying can be found in Section 4.4.2.) Porosity was calculated from Equation 4.3.

$$\boldsymbol{p = \frac{W_{ssd} - W_{dry}}{W_{ssd} - W'} * 100\%} \qquad (\mathbf{4.3})$$

where:

W_{ssd} = weight of saturated surface dry (SSD) sample in air, g

W_{dry} = weight of oven dry sample in air, g

W' = weight of saturated sample under water, g

It should be noted that the denominator of this equation is representing the volume of concrete excluding permeable voids, or the volume of the solid phase of concrete. The calculated porosity and related UPV are shown in Table 4.8 and plotted in Figure 4.6.

Table 4.8 Porosity and UPV

Sample	W_{ssd} (g)	W_{dry} (g)	W' (g)	p (%)	SSD UPV (m/s)	Dry UPV (m/s)
M1	4059.9	3957.7	2290.7	5.78	4669	4432
M2	3809.8	3698.6	2078.5	6.42	4440	4300
M3	3967.8	3845.7	2178.9	6.83	4493	4234
M4	4011.7	3904.7	2254.5	6.09	4694	4363
M5	3942.9	3832.2	2202.5	6.36	4537	4326
M6	4023.7	3918.5	2271.6	6.00	4724	4417

Note: Number of repeated UPV measurements =5

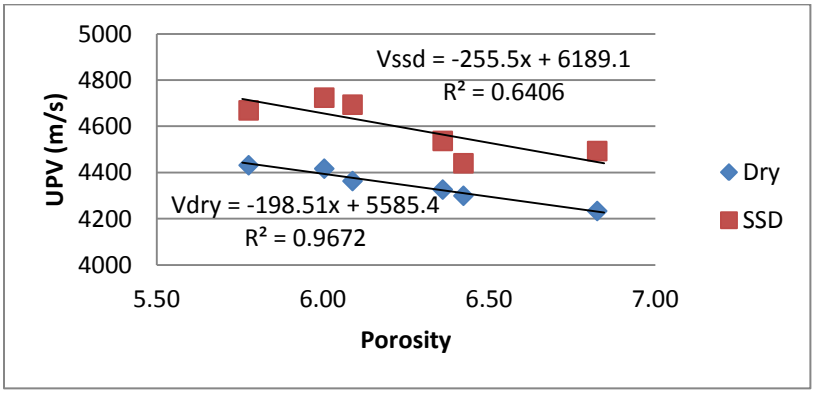

Figure 4.6 Relationship between UPV and Porosity

The outlier analysis method as described in section 3.3 was used in these samples' porosity values, and no outlier was found. From these data it can be observed that UPV at both SSD and dry conditions follow a linearly decreasing trend to porosity, similar to previous studies [24]. The regression equations for dry and SSD conditions are respectively:

$$\boldsymbol{V_{dry} = -198.5p + 5585, with\ R^2 = 0.9672} \qquad (\mathbf{4.4})$$

$$\boldsymbol{V_{ssd} = -255.5p + 6189, with\ R^2 = 0.6406} \qquad (\mathbf{4.5})$$

where V is the pulse velocity (m/s) and p is porosity (%).

It is believed that the method to measure porosity in this study is more likely to measure capillary pores and some gel pores, which Yaman et al. [24] stated are susceptible to change shape, connectivity and size, with the change of moisture. When water is absorbed, it causes swelling of the C-S-H layers and fills in the capillary pores, "elongating the channels and segmenting the pore structure", resulting in a higher variability in UPV among different samples. When concrete is dried, some of these gel pores will collapse.

4.4.4 Effects of Concrete Hardening on Ultrasonic Pulse Velocity

As discussed in Section 4.4.1, UPV shows dependency on concrete age. Since modulus and density of concrete increase with age at a decreasing rate, so is expected for UPV. Table 4.9 shows the UPV of six "control" samples on different days after casting. Since these "control" samples were kept in a water bath throughout this study, and thus without being exposed to changes in moisture producing secondary effects on porosity, the only factor impacting UPV growth is cement hydration/concrete hardening. The UPV values are plotted versus age in Figure 4.7.

Table 4.9 UPV at Different Ages (m/s) (Batch 4)

Age (days)	A	B	C	D	E	F	Mean	% Change
29	4285	4172	4119	4265	4294	4319	4242	--
35	4370	4275	4186	4289	4271	4278	4278	0.84
70	4547	4322	4344	4489	4443	4495	4440	3.78
77	4605	4449	4397	4622	4436	4640	4525	1.92
100	4566	4346	4381	4668	4565	4659	4531	0.13
114	4612	4450	4315	4554	4533	4640	4517	-0.30
122	4530	4403	4383	4555	4501	4609	4497	-0.45

Note: UPV repeatability ±1.0 %; Number of repeated UPV measurements =5

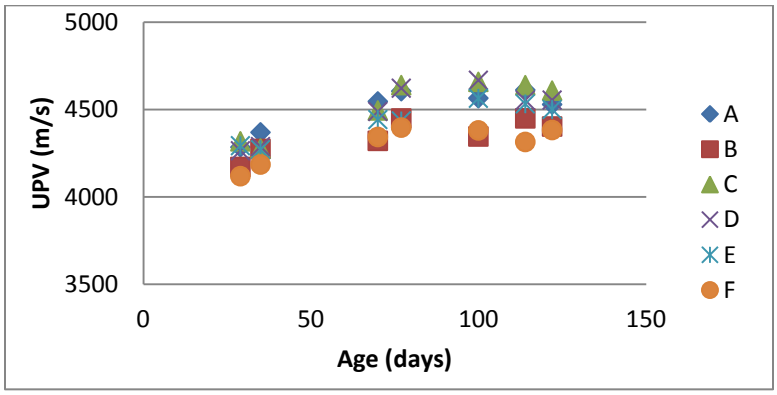

Figure 4.7 Relationship between UPV and Age for Samples A through F

The outlier analysis method as described in section 3.3 was used in these samples' initial UPV values, and no outlier was discovered. The results from 29 to 77 days showed that UPV increases with age for all samples. The UPV measurements after 77 days seemed to stabilize with some scatter (less than 0.5 %), which reflects the NDT repeatability level. Thus, it was concluded that UPV increased gradually with age and then stabilized, in accordance with past studies [33, 50]. The regression based on the average UPV of the six samples, shown in Table 4.9 and Figure 4.8 is:

$$\boldsymbol{V = 204\,ln(D) + 3569, with\ R^2 = 0.9008} \qquad \boldsymbol{(4.6)}$$

where V is the pulse velocity (m/s) and D is age (days).

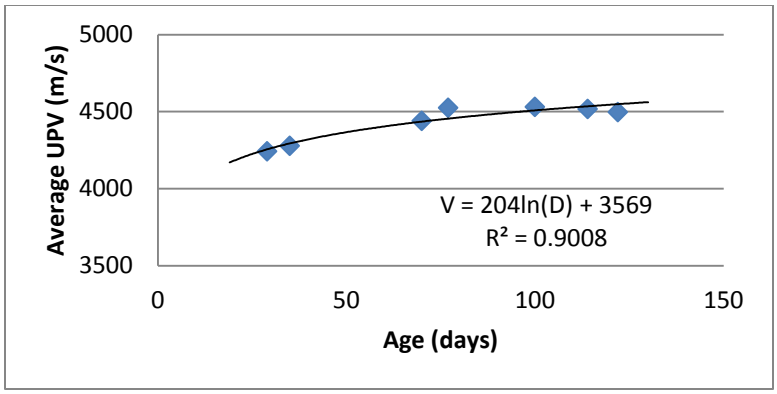

Figure 4.8 Relationship between Average UPV and Age

4.4.5 Effects of Density on Ultrasonic Pulse Velocity

In dry concrete, density of concrete is proportional to the solid fraction. In saturated concrete, density is related to the moisture content as well, and thus this should be reflected in the UPV value. Hence, the relationship between concrete density and UPV was also examined.

Density was determined according to ASTM C642, by weighing samples in air and in water and calculated according to:

$$\boldsymbol{\rho = \frac{W_{ssd}}{W_{ssd} - W'}} \qquad (\mathbf{4.7})$$

where:

ρ = measured density of concrete, g/cm^3

Wssd = weight of saturated surface dry (SSD) sample in air, g

W' = weight of saturated sample under water, g

Density was determined on the control samples from 77 days on. In addition, samples from Batch 3 were also used for 193 days. The data are shown in Table 4.10. Density was plotted against the corresponding UPV for all samples in Figure 4.9.

Table 4.10 Density and UPV

Batch	Age (days)	Sample	ρ (g/cm^3)	UPV (m/s)*
4	77	A	2.299	4605
		B	2.210	4449
		C	2.221	4397
		D	2.282	4622
		E	2.264	4436
		F	2.295	4640
	100	A	2.292	4566
		B	2.201	4346
		C	2.217	4381
		D	2.284	4668
		E	2.271	4565
		F	2.297	4659
	114	A	2.296	4612
		B	2.204	4450
		C	2.221	4315
		D	2.285	4554
		E	2.274	4533
		F	2.299	4640
3	193	1	2.313	4628
		2	2.343	4624
		3	2.374	4821
		4	2.329	4680
		5	2.351	4659
		6	2.290	4520
		7	2.321	4601

* Number of repeated UPV measurements =5

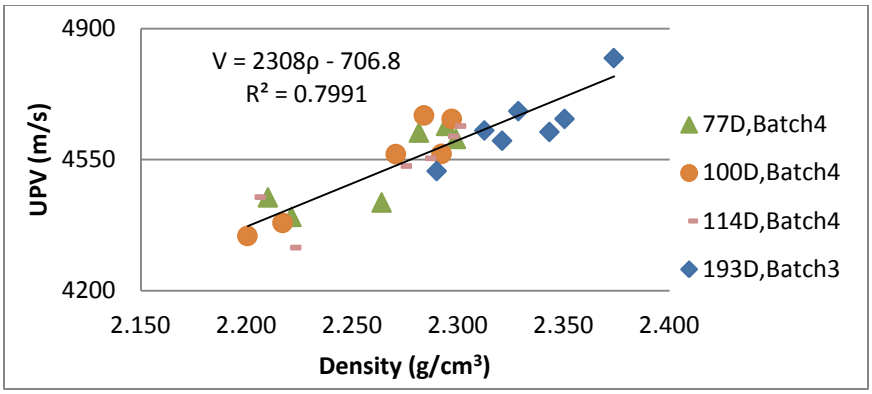

Figure 4.9 Relationship between Density and UPV

An outlier analysis method (as described in section 3.3) was used in these data and no outlier was found. Regression on both batches yielded the following regression equation:

$$\boldsymbol{V = 2308\,\rho - 706.8, with\ R^2 = 0.7991} \qquad (\mathbf{4.8})$$

where V is the pulse velocity (m/s) and ρ is density (g/cm^3). This indicates that eventually UPV and density have a good correlation after 77 days, regardless of batch.

4.4.6 Ultrasonic Pulse Velocity versus Compressive Strength and Flexural Strength

It is generally expected that UPV is increasing with compressive strength, *fc*, and flexural strength, *Mr* [34, 51, 52]. In this study, UPV was measured on compressive strength samples, as discussed in Section 4.2. The dynamic modulus, *Ed*, was calculated according to Equation 2.4. The results are shown in Table 4.11.

Table 4.11 UPV, Dynamic Modulus and Compressive Strength of Cylinders

Batch	Age (days)	Sample	Length (mm)	Transit Time (μs)	UPV (m/s)*	Ed (GPa)	fc (kPa)
4	28	1	200.279	50.8	3940	35.21	33214
		2	200.355	49.3	4062	37.36	33273
		3	198.704	50.7	3922	35.26	32854
		Mean			3974	35.95	33113
		COV (%)			1.91	3.42	0.69
1	56	1	204.368	47.2	4334	43.99	36592
		2	204.826	49.6	4128	38.85	30372
		3	205.334	50.0	4107	39.08	34210
		Mean			4189	40.64	33725
		COV (%)			2.99	7.15	9.31

* Number of repeated NDT measurements on the same sample =5

An outlier analysis method (as described in section 3.3) was used in these data and no outlier was found. It can be seen that UPV has a good relationship to compressive strength. However, such a relationship is affected by the relatively high variability in the repeatability of compressive strength testing. In this study, the presence of fibers further affects the results due to significant issues with the surface finishing characteristics of concrete, as shown in Figure 4.10. These effects are significantly pronounced for Batch 1 with 56 days. As mentioned in Section 2.6.6, some study [53] have concluded that UPV is not accurate enough to predict concrete strength.

Regarding the relationship between UPV and flexural strength, the results are shown in Table 4.12.

Figure 4.10 Top Finishing of Cylinders

Table 4.12 UPV, Dynamic Modulus and Flexural Strength of Beams

Batch	Age (days)	Sample	UPV (m/s)*	Ed (GPa)	Mr (kPa)
4	28	1	4145	38.23	4423
		2	4318	42.89	4932
		3	4268	41.83	4631
		Mean	4244	40.98	4662
		COV (%)	2.10	5.97	5.49
1	58	1	4441	45.91	5099
		2	4461	46.47	5378
		3	4458	46.74	5449
		4	4483	46.72	5128
		5	4383	44.64	4541
		6	4441	45.19	4253
		Mean	4445	45.95	4975
		COV (%)	0.76	1.89	9.58
	75	1	4407	44.81	5228
		2	4537	47.76	5190
		3	4482	46.81	4688
		Mean	4475	46.46	5035
		COV (%)	1.46	3.24	5.98

* Number of repeated NDT measurements on the same sample =5

An outlier analysis method (as described in section 3.3) was conducted in these data and no outlier was found. Beams show a satisfactory trend of relating UPV to flexural strength. By averaging the samples with the same age, a linear relationship can be fitted to flexural strength versus UPV and versus dynamic modulus, as plotted in Figure 4.11.

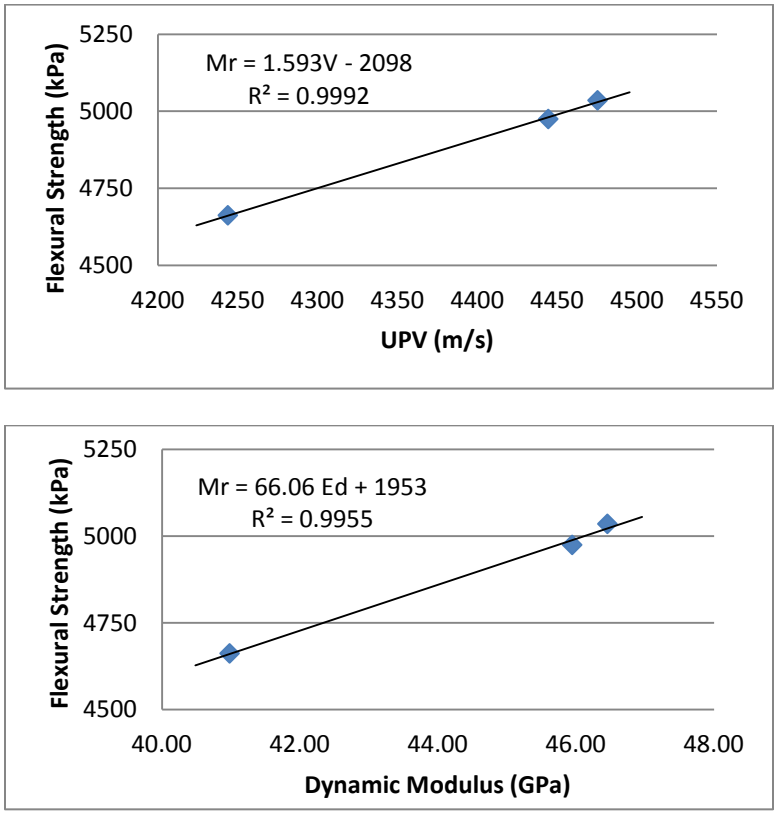

Figure 4.11 Relationship between UPV, Dynamic Modulus and Flexural Strength

The regression equations are:

$$\boldsymbol{Mr = 1.593V - 2098, with\ R^2 = 0.9992} \qquad \boldsymbol{(4.9)}$$

and

$$\boldsymbol{Mr = 66.06Ed + 1953, with\ R^2 = 0.9955} \qquad \boldsymbol{(4.10)}$$

where *Mr* is flexural strength (kPa), *V* is pulse velocity (m/s) and *Ed* is dynamic modulus (GPa).

4.4.7 Comparison of Frequencies

Wavelength, which is determined by the frequency, influences the measured UPV values, when it is comparable to aggregate size/path length. The higher the frequency is, the shorter the wavelength, the more likely the waves get attenuated, resulting in a lower UPV. This is defined as the dispersive character of concrete, reported by Popovics [34].

As noted in Section 3.2, two NDT devices were employed in this study. Model V-C-9900 was used systematically for all tests with a frequency of 54 kHz, while Model C-4902, with a frequency of 36 kHz, was used to examine whether a different frequency would provide different results. UPV was measured at the center of the cross sections. The results, along with the mean and COV, are presented in Table 4.13. An outlier analysis method (as described in section 3.3) was used in these data before analysis.

Table 4.13 UPV Measurements for 54 and 36 kHz (m/s)

Age (days)	70						114					
Sample	A	B	C	D	E	F	A	B	C	D	E	F
V-C-9900 (54 kHz)	4549	4318	4356	4496	4463	4503	4583	4444	4276	4563	4543	4668
	4549	4343	4350	4483	4463	4483	4590	4457	4307	4584	4549	4633
	4549	4324	4344	4489	4431	4490	4618	4450	4276	4536	4556	4633
	4543	4318	4344	4483	4431	4497	4632	4457	4356	4543	4489	4612
	4543	4306	4325	4496	4431	4503	4639	4444	4362	4543	4529	4654
Mean	4547	4322	4344	4489	4443	4495	4612	4450	4315	4554	4533	4640
COV (%)	0.08	0.31	0.27	0.15	0.40	0.19	0.54	0.15	0.96	0.43	0.59	0.47
C-4902 (36 kHz)	4563	4318	4313	4529	4450	4537	4597	4431	4301	4550	4476	4668
	4570	4306	4319	4529	4469	4537	4563	4444	4331	4529	4502	4690
	4516	4349	4319	4536	4463	4550	4583	4424	4331	4529	4502	4683
	4529	4349	4265	4516	4424	4537	4535	4386	4294	4529	4516	4683
	4516	4336	4283	4529	4437	4464	4522	4386	4288	4556	4509	4690
Mean	4539	4331	4300	4528	4449	4525	4560	4414	4309	4539	4501	4683
COV (%)	0.57	0.44	0.57	0.16	0.42	0.77	0.69	0.60	0.48	0.29	0.34	0.19

As it can be seen from this table, the 36 kHz frequency produced a similar repeatability to the 54 kHz, with all COV below 1 %. Also, the two frequencies produced similar results. However, in some instances, the 54 kHz produced higher transit times and vice versa. Thus, a systematical comparison of these effects was conducted using ANOVA. The level of significance is $\alpha = 0.05$. The results are shown in Table 4.14.

Table 4.14 ANOVA: Effect of Frequency and Sampling on UPV

Age (days)	*Source of Variation*	*SS*	*df*	*MS*	*F*	*P-value*	*F crit*
70	Frequency	407	1	407	1.217	0.276	4.043
	Sampling	470394	5	94079	280.9	2.6E-34	2.409
	Frequency*Sampling	10829	5	2166	6.467	1.1E-04	2.409
	Within	16077	48	335			
	Total	497708	59				
114	Frequency	4097	1	4097	7.496	8.6E-03	4.043
	Sampling	751834	5	150367	275.1	4.2E-34	2.409
	Frequency*Sampling	13807	5	2761	5.052	8.5E-04	2.409
	Within	26234	48	547			
	Total	795972	59				

The first row in Table 4.14 shows the statistics of the factor "frequency" for the 70-day case. Since the F statistic, 1.217, is lower than the F-critical 4.043 (or since P-value, 0.276, is larger than 0.025), the null hypothesis is accepted that the factor "frequency" is not significant. The second row shows the significance of the factor "sampling" for the 70-day case. Since the F statistic, 280.9, is much larger than the F-critical 2.409 (or since P-value, 2.6E-34, is much smaller compared with 0.025), the alternative hypothesis is accepted that the factor "sampling" is significant. There is also potential interaction between the two factors "frequency" and "sampling" since the third row shows a higher F statistic (6.467) than F-critical (2.409). The fourth row "within" shows the statistics related to the variations among five UPV measurements.

For the 114-day case, the factor "frequency" is significant since the F statistic, 7.496, is larger than the F-critical 4.043. The factor "sampling" is significant as well since the F statistic, 275.1, is much larger than the F-critical 2.409. Again, there is potential interaction between the two factors due to a larger F statistic (5.052) than the F-critical (2.409). It was concluded that two NDT devices are not interchangeable.

4.5 Modeling

In Section 4.4.3 it was attempted to relate porosity to dry and SSD UPV. It was observed that the relationship between UPV and porosity for dry conditions provided a good correlation, while this was not the case for SSD conditions which may be attributed to the change in pore shape, connectivity, size etc. from the presence of moisture. In this section, the effects of the amount of water within the pores on UPV were quantitatively examined by considering dry, SSD and partially saturated conditions altogether. In order to evaluate such effects, the concrete is decomposed into three phases: air, water and solid mass. The portion of the porosity filled with water, p_w, is accounted from the total porosity, p. The remaining portion is the porosity with air, or free porosity, p_a. Therefore the porosity according to Equation 4.3 is equal to:

$$\boldsymbol{p = p_w + p_a} \qquad (\mathbf{4.11})$$

where:

p = total porosity

p_w = saturated porosity

p_a = free porosity

Hence that data of Tables 4.6 and 4.8 were used to calculate the specific porosity values shown in Table 4.15.

Table 4.15 Saturated and Free Porosity versus UPV

Sample	p_w (%)	p_a (%)	UPV (m/s)*
M1	5.78	0.00 (SSD)	4669
	5.25	0.53	4679
	2.96	2.81	4531
	0.97	4.80	4532
	0.04	5.74	4485
	0.00	5.78 (Dry)	4432
M2	6.42	0.00 (SSD)	4440
	5.85	0.57	4479
	2.74	3.68	4316
	0.01	6.42	4305
	0.00	6.42 (Dry)	4300
M3	6.83	0.00 (SSD)	4493
	6.00	0.82	4435
	2.83	3.99	4309
	0.14	6.69	4253
	0.00	6.83 (Dry)	4234
M4	6.09	0.00 (SSD)	4694
	5.04	1.05	4522
	3.39	2.70	4523
	2.85	3.24	4424
	1.67	4.42	4487
	0.67	5.42	4361
	0.00	6.09 (Dry)	4363
M5	6.36	0.00 (SSD)	4537
	5.10	1.26	4533
	3.35	3.01	4429
	2.86	3.50	4431
	1.69	4.67	4418
	0.66	5.70	4372
	0.00	6.36 (Dry)	4326
M6	6.00	0.00 (SSD)	4724
	5.59	0.41	4679
	4.88	1.12	4675
	3.30	2.70	4617
	1.62	4.39	4535
	0.66	5.34	4462
	0.00	6.00 (Dry)	4417

* Number of repeated UPV measurements =5

4.5.1 Parallel System

As cited by Yaman [29], the effects of porosity on UPV was modeled by Shkolnik et al. with a linear relationship. Thus, a linear expression that considers the three phases composed of solid, air and moisture may be described as the following equation, assuming that the three phases are in parallel.

$$\boldsymbol{V = a_1 * V_{solid} * (1 - p) + a_2 * V_w * p_w + a_3 * V_a * p_a + b} \quad (\boldsymbol{4.12a})$$

where:

V = ultrasonic pulse velocity, m/s

V_{solid} = ultrasonic pulse velocity in solid concrete skeleton, assumed 5585.4 m/s from Equation 4.4

V_w = ultrasonic pulse velocity in water, assumed 1485.7 m/s as at 23.9 ℃ (75 ℉)

V_a = ultrasonic pulse velocity in water, assumed 344.1 m/s as at 23.9 ℃ (75 ℉)

a_1, a_2, a_3 and b are regression coefficients.

Using the Excel built-in tool "Regression" for multiple regression analysis on the data of Table 4.15, the following regression coefficients and statistics were obtained.

Table 4.16 Regression Results for the Parallel Model (Equation 4.12a)

	Coefficients	*Standard Error*	*t Stat*	*P-value*	*Lower 95%*	*Upper 95%*
b	-20095	2354.0	-8.536	5.69E-10	-24878.5	-15310.7
V_{solid}*(1-p)	4.67	0.4493	10.392	4.32E-12	3.756	5.582
V_w*p_w	2.54	0.2268	11.220	5.65E-13	2.084	3.005
V_a*p_a	0.00	0.00	65535.00	#NUM!	0.00	0.00

The first row of Table 4.16 provides the coefficient b, -20095, and the related statistics. Since the t-statistic, -8.536, is not inbetween but far from the 95 % range, which is -15310.7 to -24878.5 (or since P-value is much smaller than 0.025), the alternative

hypothesis is accepted that *b* is significant. The second row provides the coefficient for $V_{solid}*(1-p)$, or a_1, and the related statistics. Since the t-statistic, 10.392, is not inbetween the 95 % range, 3.756 to 5.582 (or since P-value for this parameter is very low), the alternative hypothesis is accepted that a_1 is significant. The same is true for a_2 (the t-statistic, 11.220, is not in between the 95 % range, 2.084 to 3.005) but not a_3. In fact, a_3 was found to be zero. This was expected since in Equation 4.11, p, p_w and p_a are dependent variables. In other words, once the contribution of p and p_w are determined, that of p_a is related to these values. As a result, the coefficient for p_a*V_a, or a_3, was eliminated from the regression. Therefore, Equation 4.12a was revised to Equation 4.12b, based on which multiple regression was repeated. The coefficients and statistics are shown in Table 4.17 and Equation 4.13.

$$\boldsymbol{V = a_1 * V_{solid} * (1-p) + a_2 * V_w * p_w + b} \qquad (\mathbf{4.12b})$$

Table 4.17 Regression Results for the Parallel Model (Equation 4.12b)

	Coefficients	*Standard Error*	*t Stat*	*P-value*	*Lower 95%*	*Upper 95%*
b	-20095	2354.0	-8.536	5.69E-10	-24878.5	-15310.7
Vsolid*(1-p)	4.67	0.4493	10.392	4.32E-12	3.756	5.582
Vw*pw	2.54	0.2268	11.220	5.65E-13	2.084	3.005

$$\boldsymbol{V = 4.67 * 5585(1-p) + 2.54 * 1486p_w - 20095} \qquad (\mathbf{4.13})$$

with adjusted R^2= 0.8590.

It is shown in Table 4.17 that the coefficients *b*, a_1, a_2 as well as the related statistics are the same. So the alternative hypotheses are accepted that all the three parameters are significant.

Equation 4.13 also shows that the water has a lower coefficient than the solid, which reflects possible temperature gradient from the solid to the water, uneven

distribution of water in the pores, as well as variability in the densities of the water in small-dimensioned capillaries and gel pores. The effects of this unevenness of water on UPV are also reported by Popovics [25].

4.5.2 Layered System

As proposed by Lin [27], the different phases in concrete can be modeled as layers. Thus, the following equation was proposed to integrate solid, air and water as in a layered system:

$$\frac{1}{V} = a_1 * \frac{1-p}{V_{solid}} + a_2 * \frac{p_w}{V_w} + a_3 * \frac{p_a}{V_a} + b \qquad (4.14a)$$

As discussed in the previous section, p, p_w and p_a are not independent, and thus the equation can be re-written as:

$$\frac{1}{V} = a_1 * \frac{1-p}{V_{solid}} + a_2 * \frac{p_w}{V_w} + b \qquad (4.14b)$$

The results of the multiple regression analysis are shown in Table 4.18 and the following equation.

Table 4.18 Regression Results for the Layered Model (Equation 4.14b)

	Coefficients	*Standard Error*	*t Stat*	*P-value*	*Lower 95%*	*Upper 95%*
b	0.00146	0.000114	12.846	1.33E-14	1.23E-03	1.69E-03
(1-p)/Vsolid	-7.322	0.676	-10.829	1.46E-12	-8.696	-5.948
pw/Vw	-0.280	0.024	-11.601	2.28E-13	-0.329	-0.231

$$\frac{1}{V} = -7.32 * \frac{1-p}{5585} - 0.280 * \frac{p_w}{1486} + \frac{1}{685} \qquad (4.15)$$

with adjusted R^2= 0.8678.

The coefficient *b*, 0.00146 in this model, is provided in the first row. Since the t-statistic, 12.846, is far from the 95 % range, 1.23E-3 to 1.69E-3 (or since P-value is much smaller than 0.025), the alternative hypothesis is accepted that *b* is significant. The coefficient a_1, -7.322, has a t-statistic -10.829, outside the 95 % range, -8.696 to -5.948. Thus the alternative hypothesis is accepted that a_1 is significant. Regarding a_2, the t-statistic is -11.601, far below the lower 95 % t-critical, -0.329, as a result the alternative hypothesis is accepted that a_2 is significant.

4.5.3 Exponential System

As proposed by Popovics [26] and reported in Equations 2.6 through 2.8, the effects of porosity on UPV may be modeled with an exponential relationship. The following equation was thus proposed based on this modeling approach:

$$\boldsymbol{V = V_{p0} * (1 - p_w)^{a_1} * (1 - p_a)^{a_2}} \qquad (\mathbf{4.16a})$$

or

$$\boldsymbol{ln(V) = ln(V_{p0}) + a_1 * ln(1 - p_w) + a_2 * ln(1 - p_a)} \qquad (\mathbf{4.16b})$$

where V_{p0} is the ultrasonic pulse velocity at theoretical zero porosity, m/s.

The following results were obtained from the multiple regression analysis.

Table 4.19 Regression Result for the Exponential Model (Equation 4.16b)

	Coefficients	*Standard Error*	*t Stat*	*P-value*	*Lower 95%*	*Upper 95%*
Intercept	8.725	0.034	256.7	1.75E-57	8.656	8.794
ln(1-pw)	4.591	0.534	8.596	4.83E-10	3.505	5.676
ln(1-pa)	5.403	0.533	10.141	8.13E-12	4.321	6.486

$$\boldsymbol{ln(V) = ln(6157) + 4.59ln(1 - p_w) + 5.40ln(1 - p_a)} \qquad (\mathbf{4.17})$$

with adjusted R^2= 0.8534.

The first row provides the value of lnV_{p0} and the related statistics. Since the t-statistic, 256.7, is far beyond the 95 % range, 8.656 to 8.794 (or since P-value is much smaller than 0.025), the alternative hypothesis is accepted that V_{p0} is significant. Since the coefficient a_1, 4.591, has a t-statistic 8.596, beyond the 95 % range, 3.505 to 5.676, the alternative hypothesis is accepted that a_1 is significant. Again, since the coefficient a_2, 5.403, has a t-statistic 10.141, higher than the upper 95 % t-critical, 6.486, the alternative hypothesis is accepted that a_2 is significant as well.

With this model, the V_{p0} is extrapolated to be 6157 m/s, which is higher than the value previously estimated in this study (5585 m/s). Hence this model should be used with great care.

4.6 Discussion and Conclusion

In this chapter, the repeatability of UPV measurement was first assessed. Then the impacts of concrete properties and environmental conditions on UPV were examined. As it can be concluded, UPV in concrete is not only dependent on the concrete properties like moisture level, concrete age, density etc, but also influenced by transducer location and ultrasonic wave frequency. The relationships between UPV and absorption, porosity, compressive and flexural strength etc. of the concrete for this specific mixture were established. Because concrete, and especially polypropylene fiber reinforced concrete in this study, is a highly heterogeneous composite material, variability in concrete properties is higher than in UPV.

One of the major effects in UPV measurements is the presence of water and voids into the concrete. Thus three alternative approaches of modeling the moisture content within concrete pores were examined in relation to the potential effects on UPV. With these models, UPV can be determined, in function with the porosities in concrete (total, water-filled and free), by measuring the existing and the maximum possible amounts of water in the samples.

5 Fatigue and Ultrasonic Pulse Velocity

5.1 Introduction

Theoretically, the change of microstructure or the development of cracks can impact pulse propagation within concrete. Hence, ultrasonic pulse velocity (UPV) should be able to detect progressive cracking due to fatigue.

An artificially cut sample and a cracked sample under loading were studied to find the sensitivity of UPV and determine the best scheme for UPV testing setup before fatigue was studied.

5.2 Alternative Transducer Contact Types with "Direct Arrangement"

As introduced in Section 2.5.4, the "direct arrangement" is the most satisfactory among the three transducer arrangements (direct, semi-direct and indirect), since it receives the maximum pulse energy and obtains the most accurate UPV. Within "direct arrangement", different contact types with different contact areas between transducers and concrete can be used. In order to determine the best setup to assess the response of UPV to fatigue cracking, a 4-mm (0.15-inch) wide notch was initiated in the middle of a beam, which was further cut with a saw to different depths at perpendicular angle. UPV was measured at each cut depth.

5.2.1 "Full Contact"

In "full contact", the periphery of the transducers is tangent to the two sides of the concrete beam, whose length is the pulse travel distance. Corners 1 and 4, representing

the bottom and top of the beam during casting, were chosen to be measured, as shown in Figure 4.2. UPV values from the two corners were averaged to represent the UPV of the whole sample. The results are shown in Table 5.1 and plotted in Figure 5.1. An outlier analysis method (as described in section 3.3) was conducted in the repeated data before analysis and no outlier was detected.

Table 5.1 Transit Time with "Full Contact"

Cut Depth (mm)	Corner	Transit Time (μs)					Mean (μs)	UPV (m/s)	Average UPV (m/s)
0	1	66.8	66.5	66.6	66.8	67.2	66.8	4568	4510
	4	68.5	68.6	68.4	68.2	68.9	68.5	4452	
14.5	1	67.7	67.8	67.2	67.1	66.7	67.3	4532	4512
	4	68.5	68.0	67.8	67.8	67.4	67.9	4492	
29.5	1	68.1	67.9	68.5	67.8	68.2	68.1	4479	4421
	4	70.6	70.9	69.4	69.5	69.2	69.9	4363	
49.5	1	69.9	69.2	69.1	68.7	68.2	69.0	4419	4323
	4	72.2	71.4	71.4	73.5	72.4	72.2	4226	
67.5	1	76.4	75.5	76.6	76.1	75.8	76.1	4009	4128
	4	71.8	72.0	71.8	72.1	71.5	71.8	4246	

Note: Corner 1 is bottom during casting and Corner 4 is top during casting

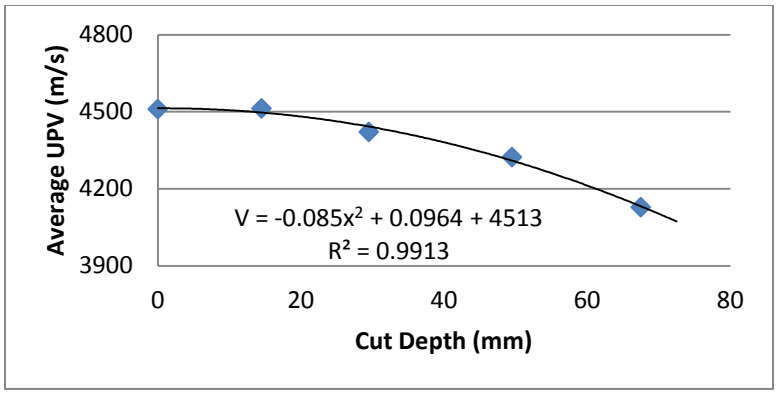

Figure 5.1 Average UPV and Cut Depth with "Full Contact"

The UPV values before any notch and at 14.5 mm notch did not show much difference. After the cut notch depth passed 14.5 mm, UPV started to decrease with an almost linear trend, fitted as:

$$\boldsymbol{V(f) = -0.085x^2 + 0.096x + 4513, with\ R^2 = 0.9913} \qquad (\mathbf{5.1})$$

where *V(f)* is ultrasonic pulse velocity (m/s) with "full contact" and *x* is the cut depth (mm).

5.2.2 "Partial Contact"

Besides the "full contact", "partial contact" was examined in this study as well. In this situation, two wooden cushions were placed underneath the concrete beam to lift it to a certain height. Transducers were placed at the same workbench as the cushion so there would be just a part of the transducers in contact with the beam surface. In "partial contact 1", the beam was lifted by about 12.7 mm. Since the diameter of the transducer is 50.8 mm, the upper 38.1 mm of the transducer was in contact to the beam. In "partial contact 2", the beam was lifted by 25.4 mm so there was just half of the transducer contacting the beam. The test at Corner 1 is shown in Figure 5.2.

UPV was measured at each cut depth similarly to the "full contact" case discussed in the previous section. The results for the two "partial contact" situations are shown in Tables 5.2 and 5.3, respectively. An outlier analysis method (as described in section 3.3) was used in the repeated data before analysis and no outlier was detected.

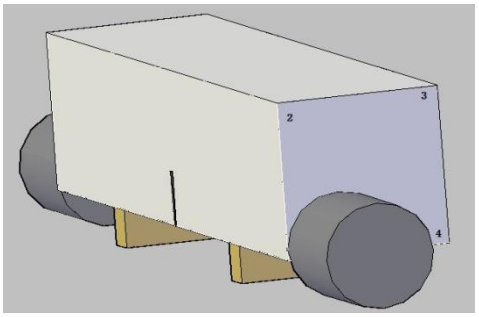

Figure 5.2 “Partial Contact” (Measured at Corner 1)

Table 5.2 Transit Time with “Partial Contact 1”

Cut Depth (mm)	Corner	Transit Time (μs)					Mean (μs)	UPV (m/s)	Average UPV (m/s)
0	1	67.6	66.5	66.1	66.1	66.2	66.5	4587	4562
	4	67.4	67.3	67.3	67.3	66.8	67.2	4538	
14.5	1	66.2	65.9	65.9	66.0	65.9	66.0	4623	4603
	4	67.6	66.9	66.1	66.0	66.2	66.6	4583	
29.5	1	67.5	66.9	67.4	67.2	66.9	67.2	4540	4460
	4	70.2	69.9	69.7	69.3	69.1	69.6	4380	
49.5	1	68.7	68.2	68.2	68.1	68.3	68.3	4466	4391
	4	71.8	70.8	70.2	70.2	70.4	70.7	4316	
67.5	1	76.0	76.0	75.5	75.3	74.7	75.5	4040	4105
	4	73.2	72.8	73.3	73.7	72.8	73.2	4169	

Note: Corner 1 is bottom during casting and Corner 4 is top during casting

Table 5.3 Transit Time with “Partial Contact 2”

Cut Depth (mm)	Corner	Transit Time (μs)					Mean (μs)	UPV (m/s)	Average UPV (m/s)
0	1	66.8	66.7	66.5	66.6	67.2	66.8	4569	4568
	4	67.6	66.9	66.6	66.5	66.4	66.8	4566	
14.5	1	67.9	67.8	67.8	68.1	67.2	67.8	4502	4546
	4	66.9	66.7	66.3	66.3	66.1	66.5	4590	
29.5	1	72.9	71.8	72.3	73.1	72.4	72.5	4207	4261
	4	70.7	70.5	70.8	70.5	71	70.7	4314	
49.5	1	72.6	72.2	71.4	71.9	72.2	72.1	4233	4241
	4	71.9	71.6	71.4	71.9	72.2	71.8	4248	
67.5	1	73.9	73.7	73.4	73.3	73.4	73.5	4148	4072
	4	76.4	76.4	76.2	76.2	76.4	76.3	3997	

Note: Corner 1 is bottom during casting and Corner 4 is top during casting

Under the "partial contact", UPV decreased significantly after the cut depth was larger than 14.5 mm. It can also be seen from Tables 5.1 through 5.3 that UPV from "partial contact 2" decreased faster than "partial contact 1", which in turn decreased faster than "full contact", indicating a higher dependency on cut depth with lower contact surface area between the transducer and the sample.

The relationships between UPV and cut depth were plotted in Figures 5.3 and 5.4.

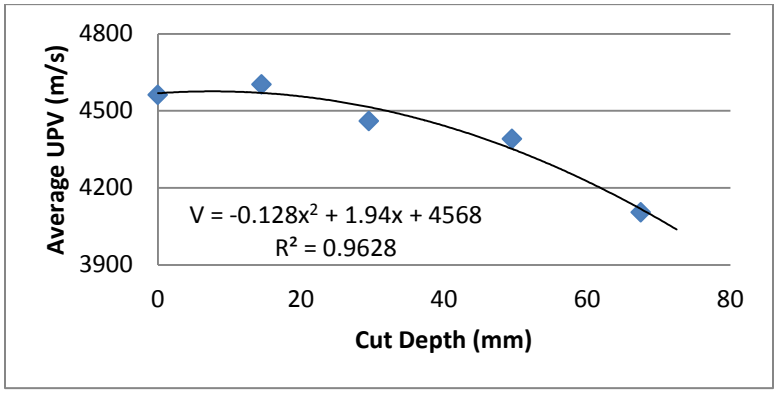

Figure 5.3 Average UPV and Cut Depth with "Partial Contact 1"

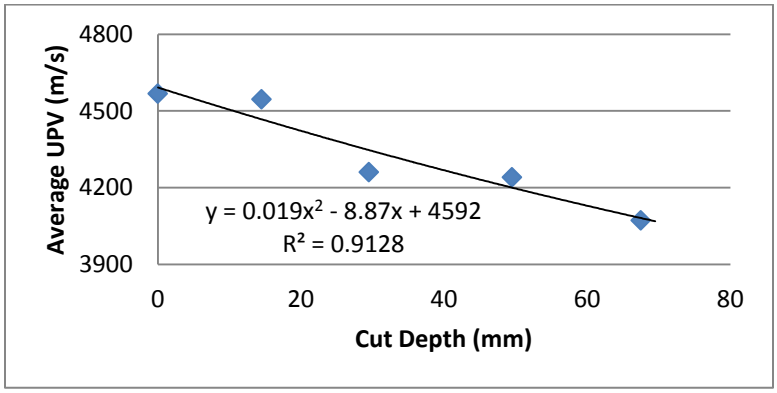

Figure 5.4 Average UPV and Cut Depth with "Partial Contact 2"

The regression curves for these two situations are

$$\boldsymbol{V(P1) = -0.128x^2 + 1.94x + 4569, with\ R^2 = 0.9628} \qquad (5.2)$$

and

$$\boldsymbol{V(P2) = -0.019x^2 - 8.87x + 4592, with\ R^2 = 0.9128} \qquad (\mathbf{5.3})$$

where *V(P1)* and *V(P2)* are ultrasonic pulse velocities (m/s) with "partial contact 1" and "partial contact 2", respectively, and *x* is the cut depth (mm).

5.2.3 Comparison of Contact Types

Since all contact types were able to detect cracking, it was important to examine the significance of "contact". Thus, the transit times measured from the three contact types at five cut depths and at two corners were analyzed with ANOVA. The following hypotheses were used:

H_0: $t_1=t_2=\ldots=t_{150}$;

H_1: at least one transit time is different

in which t_1, t_2,…, t_{150} are the individual transit time readings in Tables 5.1 through 5.3. The null hypothesis is that none of the factors, i.e. "cut depth" "contact type" or "corner", affects the transit time. The level of significance is $\sigma=0.05$, and the results are shown in Table 5.4.

Table 5.4 ANOVA: Effect of Contact Type, Cut Depth and Corner on Transit Time

Source of Variation	*SS*	*df*	*MS*	*F*	*F-critical*	*P-value*
Contact Type	48.86	2	24.431	123.305	3.072	<.0001
Cut Depth	1115.42	4	278.855	1407.409	2.447	<.0001
Corner	6.70	1	6.699	33.812	3.920	<.0001
Contact Type*Cut Depth	56.93	8	7.117	35.919	2.016	<.0001
Contact Type*Corner	5.41	2	2.705	13.652	3.072	<.0001
Cut Depth*Corner	38.91	4	9.728	49.098	2.447	<.0001
Contact Type*Cut Depth*Corner	112.57	8	14.072	71.021	2.016	<.0001
Within	23.78	120	0.198			
Total	1408.58	149				

Table 5.4 shows that the factor “contact type” has an F-statistic, 123.305, larger than the F-critical, 3.072. Thus, the null hypothesis was rejected and the factor “contact type” is significant, signifying a significant difference between “full contact” and “partial contact”. Therefore, the three contact types could not be used interchangeably. For the factor “cut depth”, since 1407.409 is larger than 2.447, it indicates that UPV is sensitive to the cut. The same is valid for the factor “corner”, since 33.812 is larger 3.920, in agreement with Section 4.4.1. The last but one row “within” shows the variability within the five transit time readings under each condition.

Besides, “contact type” seemed to interact with both “cut depth” and “corner”, as indicated by the fourth and fifth rows, as 35.919 is larger than 2.016 and 13.652 is larger than 3.072.

As a result, the “full contact” was preferred due to the accuracy of results as well as the simplicity of setting up.

5.3 Ability of Ultrasonic Pulse Velocity to Detect Cracking Due to Loading

Although UPV had been proved able to detect a 4-mm wide straight cut perpendicular to the beam, it was necessary to examine the ability of UPV to detect cracking caused by loading. Thus, a beam from Batch 1 was sawed with a very shallow notch, of about 2 mm wide and 1 mm deep, at the middle. The beam was then loaded gradually up to 75.620 kN. The resulting crack was about 70 mm long. Then the UPV was measured with “full contact”, at Corners 1 and 4 (bottom and top during casting). Transit times before and after the formation of the crack were obtained and shown in

Table 5.5. An outlier analysis method (as described in section 3.3) was conducted in the repeated data before analysis.

Table 5.5 Transit Time Before and After Cracking Due to Loading

Crack Depth (mm)	Corner	Transit Time Readings (μs)					Mean (μs)	COV(%)
0	1	70.1	69.7	70.3	68.8	69.1	69.6	0.9
	4	70.2	71.4	71.5	72.9	71.5	71.5	1.3
70	1	80.5	80.4	80.8	81.1	82.5	81.1	1.0
	4	92.6	91.6	95.7	91.7	87.1	91.7	3.4

UPV was found to be sensitive to the presence of cracking due to loading, since there was a significant increase in transit time after cracking. In addition, a slightly larger variability was observed for the cracked sample, implying the interference of crack with wave propagation. Therefore, fatigue testing was used in the following analysis.

5.4 Fatigue Test

Next, the possibility of using UPV for crack detection under fatigue testing was examined. Concrete beams were tested with cyclic fatigue loading. The stress ratio was set at 0.75 with a frequency of 5 Hz. The test parameters and results of five samples are listed in Table 5.6. An outlier analysis method (as described in section 3.3) was employed in these data and no outlier was found.

Table 5.6 Testing Parameters and Fatigue Life

Sample	1	2	3	4	5
Flexural Strength (kPa)*	4937	4937	4937	4937	4937
Stress ratio	0.75	0.75	0.75	0.75	0.75
Min Load/Max Load	0.1	0.1	0.1	0.1	0.1
Mass in Air (g)	4199.0	4178.8	4189.5	4119.7	4109.9
Mass in Water (g)	2384.2	2391.8	2392.9	2342.6	2338.6
Volume (cm3)	110.75	109.05	109.64	108.45	108.09
Length (mm)	305.054	305.003	304.978	305.054	304.876
Depth (mm)	76.784	76.606	76.505	76.403	76.302
Width (mm)	77.478	76.481	77.001	76.247	76.144
Max Load (kN)	7.398	7.269	7.299	7.209	7.180
Min Load (kN)	0.740	0.727	0.730	0.721	0.718
Mid point (kN)	4.069	3.998	4.015	3.965	3.949
Amplitude (kN)	3.329	3.271	3.285	3.244	3.231
Fatigue Life (No. of cycles)	29100	41260	30700	42380	20100

*Flexural strength was the average of all the samples from Batch 1:
5099,5378,5449,5128,4541,4253,5228,5190,4688,3961,4981,5254,5029

The fatigue life showed a great variability among samples. The COV of the five fatigue lives is 28.3 %.

5.5 Fatigue Cycle and Ultrasonic Pulse Velocity

The test was carried out as follows: UPV was measured before the fatigue loading and at different intervals during fatigue. The testing intervals were chosen based on the sample's fatigue performance and the number of cycles already applied, since fatigue damage develops faster and faster towards failure. Usually after 20,000 cycles, UPV was measured at intervals of 1000, 500 or fewer cycles depending on the sample. The results for Sample 4 in Table 5.6 are presented in Table 5.7 and Figure 5.5. (Samples 1, 2, 3 are shown in the Appendix. UPV was not measured on Sample 5 before failure.) An outlier analysis method (as described in section 3.3) was conducted in these data.

Table 5.7 UPV and Fatigue Cycles of Sample 4 (s/Mr=0.75, 5 Hz)

Cycle No.	Corner	Transit Time (μs)					Mean (μs)	UPV (m/s)	Average UPV (m/s)	% Change
25000	1	64.7	66.0	65.7	66.4	67.1	66.0	4624	4591	--
	4	67.1	67.0	66.7	66.8	67.0	66.9	4557		
30000	1	65.3	65.4	66.0	65.6	66.1	65.7	4645	4570	-0.46
	4	68.4	67.9	67.5	67.7	67.8	67.9	4494		
32000	1	66.0	66.3	66.1	66.7	66.6	66.3	4599	4516	-1.18
	4	68.5	69.2	68.0	69.5	68.8	68.8	4433		
33000	1	66.5	65.8	66.7	66.2	66.1	66.3	4605	4529	0.29
	4	68.2	69.7	68.1	68.4	68.0	68.5	4454		
34000	1	67.8	67.3	67.6	67.3	67.3	67.5	4523	4522	-0.15
	4	67.9	67.3	67.7	67.1	67.2	67.4	4522		
35000	1	66.0	66.9	66.9	66.5	66.6	66.6	4583	4517	-0.13
	4	68.5	68.4	68.6	68.5	68.6	68.5	4451		
36000	1	65.8	65.9	66.4	68.6	67.1	66.8	4570	4569	1.16
	4	68.2	67.9	68.9	67.8	67.8	68.1	4568		
37000	1	65.6	66.7	67.2	67.1	68.5	67.0	4479	4484	-1.87
	4	67.1	68.1	68.2	68.1	68.2	67.9	4489		
40000	1	67.1	67.4	67.5	67.3	67.4	67.3	4531	4496	0.27
	4	67.7	68.2	68.5	68.6	68.8	68.4	4461		
42380	Failure									

Note: Corner 1 and Corner 4 are bottom and top during casting, respectively

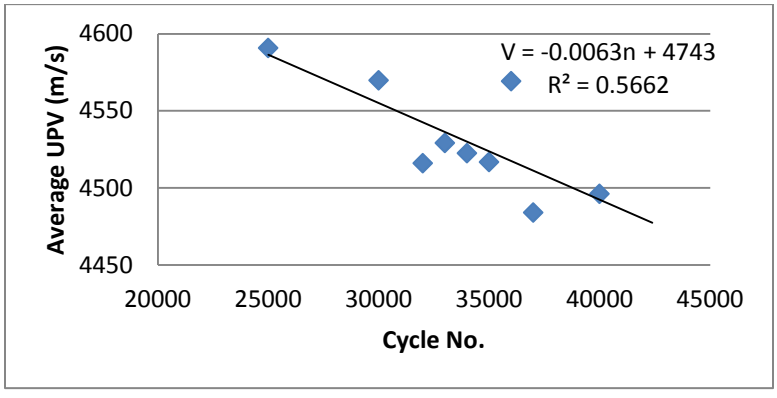

Figure 5.5 UPV with Fatigue Cycles for Sample 4

As expected, UPV decreased with fatigue cycles. However, a significant scatter was observed in the trend, which is eventually associated with the high variability in fatigue testing, due to a series of effects including testing error, sample to sample variability and sample flaws, and the effects of loading/unloading on the changing microstructure of concrete .

Because of the high variability, it was challenging to predict what the fatigue life of each sample was going to be. In addition, without the prediction of fatigue life, it was difficult to intensify the UPV testing and capture the change in transit time, since cracking propagates at a very fast rate in the last stages of fatigue. Furthermore, moving a significantly damaged sample from the fatigue pedestal for running the UPV testing became problematic for possible disintegration or further cracking of the sample. Finally, it is questionable whether UPV can detect smaller cracks developed during progressive fatigue, although it was proved able to detect a large crack.

As a result, the use of UPV for damage detection under fatigue testing was not acceptable.

5.6 Discussion and Conclusion

In this chapter, different transducer contact types for UPV testing were examined and compared. All of these setups indicated that UPV is promising in detecting an artificial cut beyond a certain size. The “full contact” was preferred based on the accuracy of results, the ease/simplicity of testing and the high receiving energy. The use of UPV for detecting fatigue cracking has been problematic due to i) the high variability inherent in fatigue testing of materials, ii) the logistics of detecting and carrying out UPV

testing at the proper intervals during fatigue testing, and iii) the limitations of UPV to detect smaller cracks.

It is believed that a more thorough understanding and modeling of the fatigue failure mechanism, especially for fiber reinforced concrete, is needed before the UPV technique can be applied for fatigue damage detection.

6 Freeze-Thaw and Ultrasonic Pulse Velocity

6.1 Introduction

Freeze-thaw testing was conducted according to ASTM C666. The temperature ranges between -17.8 ℃ and 4.4 ℃ (0 and 40 ℉). Each cycle takes roughly 4 hours, 3 hours for freezing and 1 hour for thawing. Since the freeze-thaw chamber employed in this study has 18 containers including one for a control sample to monitor and control the temperature, altogether 17 beams were studied for freeze-thaw testing. Ultrasonic pulse velocity (UPV) was measured through the freeze-thaw testing.

6.2 Measurement Procedure

Before freeze-thaw exposure the initial properties of the beam samples were measured in saturated surface dry (SSD) condition at room temperature (23.9 ℃ or 75 ℉), including the weight, the length and the initial transit time. After every 25 freeze-thaw cycles of exposure, the weight in air and UPV were measured, the samples were rotated 90 °clockwise and moved to the right by four positions in the freeze-thaw chamber. The details are as follows:

1) When freeze-thaw testing was interrupted at the thawing temperature of 4.4 ℃, the samples were kept in the freeze-thaw chamber for one day until all the ice surrounding the samples was melted.

2) After the ice was melted, the samples were transported to a water bath in an environmental chamber with a temperature of 4.4 ℃.

3) The samples were kept in the environmental chamber for at least 12 hours to make sure ice in the pores was also melted.

4) The samples were then moved out of the environmental chamber, one at a time, and dried with a towel to remove the surface moisture.

5) Length, weight in the air, and transit time were then measured. The weight in the water was finally measured.

6) Each sample was quickly put back into the water bath and placed back into the environmental chamber at 4.4 ℃.

7) After all the tests were completed, some of the samples were placed into a water bath at the room temperature for later use. These represent: Samples 4, 7, 10, 13 and 16, after 100 cycles; Samples 2, 6, 11 and 15, after 200 cycles; Samples 1, 5, 9 and 14, after 300 cycles; and the rest, after 400 cycles.

Great care was exercised during this procedure to protect the samples from moisture loss or temperature fluctuations.

6.3 Weight Change during Freeze-Thaw Testing

The weight of the SSD samples in air, W_{ssd}, was measured throughout the freeze-thaw testing at intervals of 25 cycles. The results are presented in Table 6.1. Visible scaling was observed on the lateral surface of the beams after 75 cycles and on the cross section at about 300 cycles. An outlier analysis method (as described in section 3.3) was used in these samples' initial properties and no outlier was observed.

Table 6.1 Weight with Freeze-Thaw Cycles (g)

Age (days)	29	41	51	58	65	70	77	86	93	100	107	116	122	128	135	142
Cycle No. / Sample	0	50	75	100	125	150	175	200	225	250	275	300	325	350	375	400
1	3975.5	3977.3	3978.2	3977.2	3975.9	3973.5	3972.8	3973.0	3973.0	3972.4	3968.2	3968.0				
2	4019.0	4021.9	4024.5	4024.2	4023.2	4018.6	4015.9	4011.9								
3	4007.0	4007.2	4009.2	4010.0	4011.0	4008.9	4005.8	4005.3	4006.0	4003.1	4002.8	4000.5	3997.5	3996.1	3994.9	3992.7
4	3854.9	3855.6	3857.9	3859.2												
5	4077.2	4076.4	4077.2	4076.7	4074.2	4072.1	4072.6	4072.7	4071.7	4069.6	4066.1	4061.2				
6	4010.3	4010.2	4013.3	4013.4	4012.8	4012.7	4006.9	4007.6								
7	4029.9	4031.3	4034.2	4036.3												
8	4117.1	4119.8	4122.6	4123.2	4121.5	4119.6	4117.7	4120.2	4118.6	4116.7	4112.6	4112.4	4106.0	4103.7	4099.0	4095.4
9	3950.7	3951.5	3952.6	3952.9	3948.7	3947.5	3944.6	3945.9	3943.8	3941.4	3936.0	3935.8				
10	4037.8	4041.8	4045.5	4045.7												
11	3943.9	3947.0	3948.8	3948.6	3946.7	3945.0	3945.7	3945.4								
12	3900.4	3904.1	3907.4	3905.2	3903.1	3898.8	3897.5	3899.0	3896.3	3891.4	3886.6	3878.0	3871.1	3869.4	3867.5	3866.4
13	3953.3	3955.7	3957.4	3957.7												
14	3949.9	3954.2	3957.2	3958.6	3956.9	3953.7	3949.4	3949.4	3947.0	3946.2	3945.7	3943.0				
15	3931.1	3935.7	3939.6	3941.3	3941.8	3938.8	3940.4	3939.6								
16	3972.8	3975.3	3976.9	3977.8												
17	3912.5	3915.0	3916.8	3918.0	3919.5	3917.8	3917.7	3915.4	3913.5	3911.0	3908.5	3908.0	3904.0	3900.3	3896.3	3890.6
Mean	3979.0	3981.2	3983.5	3983.9	3986.3	3983.9	3982.3	3982.1	3983.7	3981.5	3978.3	3975.9	3969.7	3967.4	3964.4	3961.3

As shown from these results, the weight increased up to a certain number of cycles, and then a reduction was observed. For example, Samples 4, 7, 10, 13 and 16, which were exposed up to 100 cycles, experienced continuous weight increase. Samples 1, 2, 11 and 12 had a weight increase up to 75 cycles, and then a reduction. The weight of Samples 8, 9 and 14 experienced a weight decrease from 125 cycles, while Samples 3, 15 and 17 from 150 cycles.

Eventually the increasing trend in weight coincides with the critical saturation theory [54], which indicates water uptake and absorption into the pore network can last for an initial period without damaging the concrete, as long as the saturation is below the critical degree, defined as where the hydraulic pressure caused by the resistance to the flow of displaced water exceeds the strength of the paste in concrete [15]. This implies that at the initial stages/cycles of freezing and thawing, although the samples were supposed to be "saturated", there was still room in the pore network for extra water, eventually explaining the increase in W_{ssd}. With more freeze-thaw cycles of exposure, internal cracking is initiated and even more water is absorbed, which will freeze later and create additional damage. On the other hand, scaling lessens the measured W_{ssd}. As a result, these two factors, the increase of absorbed water and the scaling, take place at the same time, causing the increasing/decreasing effect on the measured weight.

Due to the nature of concrete and the way of determining the SSD condition, some scatters in the results are expected. For example, Sample 6 had 0.1 g of weight decrease in the first 50 cycles, within the margin of error for weight measurements, so such changes are considered negligible. Also, variability among the samples was

observed, which is related to the variable exposure that samples undergo from one location to the next within the freeze-thaw chamber.

Examples of the weight plots of four samples, as well as the plot of the mean values of all 17 samples are shown in Figure 6.1.

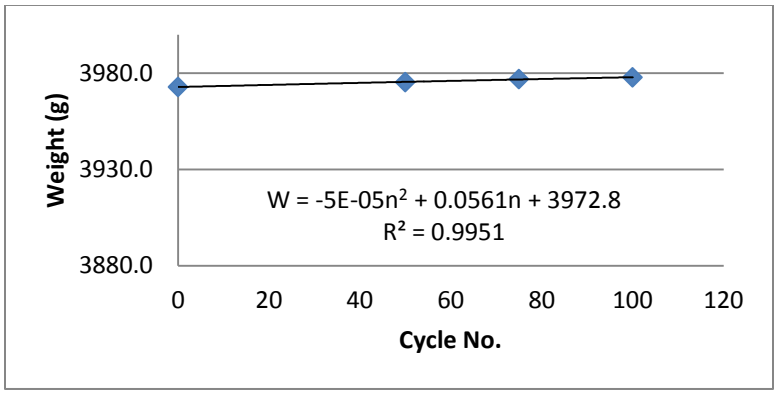

a) Sample 16

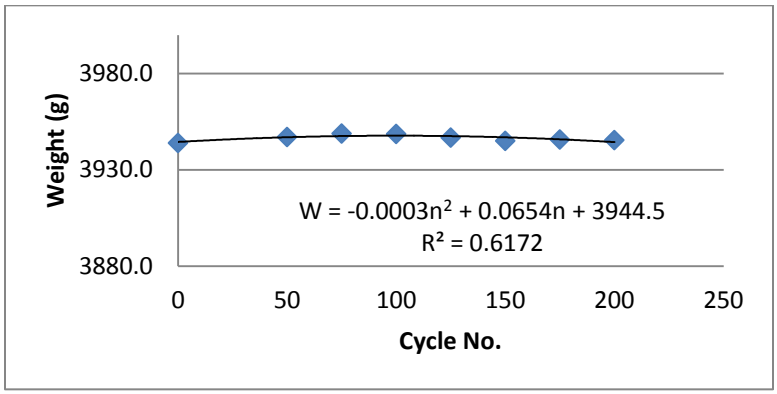

b) Sample 11

Figure 6.1 Weigh with Freeze-Thaw Cycles

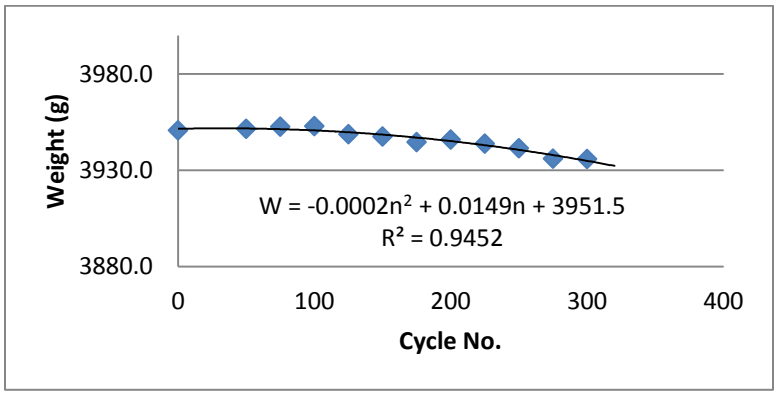

c) Sample 9

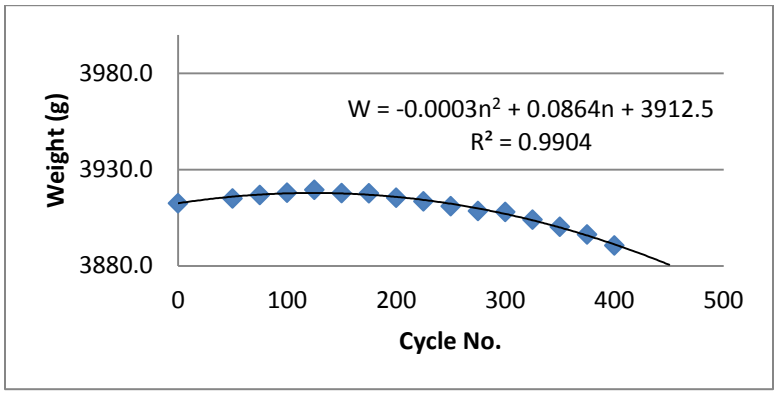

d) Sample 17

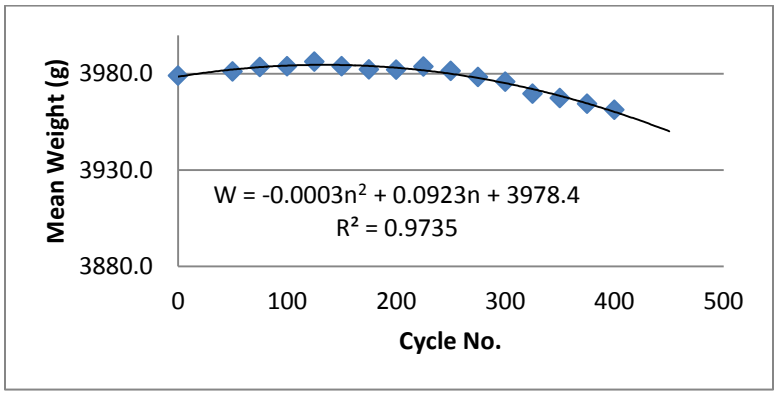

e) Mean Weight of 17 Samples

Figure 6.1 Weigh with Freeze-Thaw Cycles (Continues)

6.4 Ultrasonic Pulse Velocity Change with Freeze-Thaw Exposure

UPV was measured at every 25 cycles. Since the initial UPV was measured on samples taken out of the 23.9 ℃ (75 ℉) water bath, it needs to be adjusted to the value at 4.4 ℃ (40 ℉). In order to find the difference between these two temperatures, three 120-day samples from Batch 4 were kept in the water baths at each temperature for over 50 hours, and UPV was measured. The results are shown in the following table. An outlier analysis method (as described in section 3.3) was used before analysis.

Table 6.2 UPV at Two Temperatures

Sample	4.4 ℃ (40 ℉)	23.9 ℃ (75 ℉)	% Increase	Mean (%)
T1	4539	4622	1.831	
T2	4431	4507	1.723	1.594
T3	4604	4660	1.229	

As a result, the UPV values at 23.9 ℃ (75 ℉) was estimated to be 1.594 % higher. The UPV results at all cycles are shown in Table 6.3. The outlier analysis method, as described in section 3.3, was used in these samples' initial UPV values and no outlier was observed

Table 6.3 UPV with Freeze-Thaw Cycles (m/s)

Age (days)	29 (23.9 ℃)	29 (4.4 ℃)	41	51	58	65	70	77	86	93	100	107	116	122	128	135	142
Cycle No. / Sample	0	0	50	75	100	125	150	175	200	225	250	275	300	325	350	375	400
1	4293	4226	4306	4391	4424	4471	4459	4469	4468	4446	4320	4327	4295				
2	4316	4249	4497	4558	4613	4592	4581	4511	4546								
3	4304	4236	4461	4497	4495	4462	4455	4476	4483	4436	4385	4421	4307	4371	4314	4299	--
4	4219	4153	4435	4395	4417												
5	4334	4266	4580	4613	4555	4559	4629	4541	4566	4486	4492	4463	4360				
6	4320	4252	4349	4407	4425	4340	4396	4383	4411								
7	4150	4085	4428	4355	4476												
8	4245	4178	4495	4587	4627	4578	4649	4555	4561	4489	4481	4441	4368	4400	4411	4356	4458
9	4326	4258	4543	4525	4578	4555	4500	4590	4503	4537	4463	4466	4345				
10	4205	4139	4477	4428	4508												
11	4252	4186	4449	4437	4550	4523	4425	4497	4468								
12	4267	4200	4427	4502	4518	4445	4404	4422	4503	4321	4361	4320	4279	4190	4331	4232	4193
13	4269	4202	4496	4501	4601												
14	4191	4125	4429	4473	4484	4376	4333	4371	4453	4363	4379	4311	4270				
15	4269	4202	4376	4398	4435	4385	4388	4393	4425								
16	4264	4197	4489	4545	4540												
17	4303	4235	4414	4412	4431	4407	4454	4431	4387	4348	--	4315	4294	4228	4296	4135	4172
Mean	4266	4199	4450	4472	4510	4474	4473	4470	4481	4428	4412	4383	4315	4297	4338	4256	4309
COV (%)	1.21	1.21	1.53	1.71	1.56	1.93	2.22	1.60	1.29	1.74	1.50	1.61	0.88	2.42	1.16	2.24	3.73

Note: All were measured at 4.4 ºC except the 29-day; number of repeated UPV measurements = 5

The trend of UPV generally follows that of the weight, which increased up to a certain number of cycles, and then decreased. For example, Samples 4, 7, 10 and 11 experienced a UPV increase up to 50 cycles. Samples 2, 6, 8, 9, 12, 14, 15 and 17 had a UPV increase until 100 cycles followed by a decrease. UPV of Sample 1 started to decrease from after 125 cycles. Such trends were expected based on the critical saturation theory: the pore network absorbs water in the initial period of freeze-thaw testing to accelerate pulse propagation, and is enlarged later on due to cracking and decreases UPV.

Although this trend was expected, some scatters are observed. This perhaps reflects the potential errors in length measurements. However, such phenomenon could also reflect the combined effects from the increase in the amount of absorbed water and from the porosity change due to freeze-thaw cracking. Such effects are difficult to separate, and thus it was not possible to further examine them respectively within this research. As mentioned previously, the exposure variations from one location of the freeze-thaw chamber to another may be another reason for observing such scatters (and thus variability on weight measurements).

Example trends for four samples, as well as the mean UPV values are plotted in Figure 6.2.

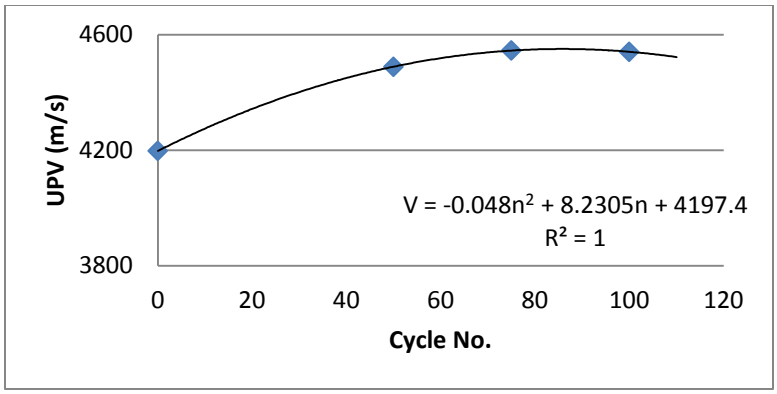

a) Sample 16

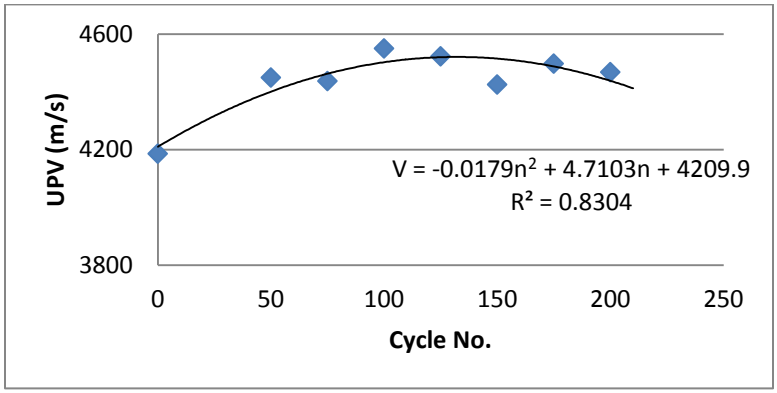

b) Sample 11

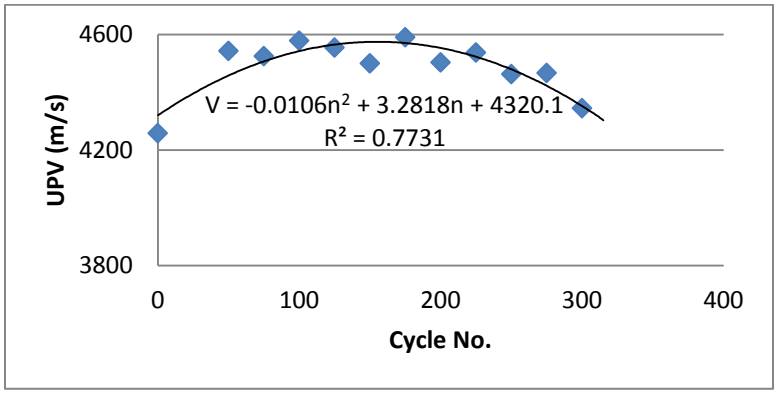

c) Sample 9

Figure 6.2 UPV with Freeze-Thaw Cycles

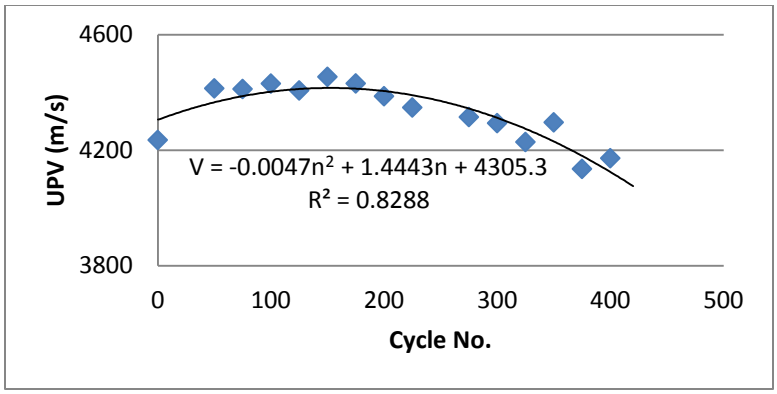

d) Sample 17

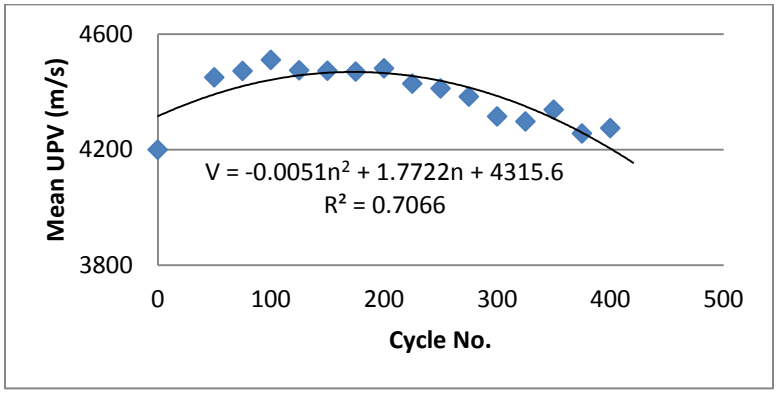

e) Mean UPV Values of 17 Samples
Figure 6.2 UPV with Freeze-Thaw Cycles (Continues)

From Figure 6.2e, it can be observed that the mean UPV reached the peak at about 100 cycles, stayed at that level to 200 cycles, and then decreased as the number of freeze-thaw cycles increased. Such trend supports the possibility that UPV increases during the initial freeze-thaw cycles as the amount of absorbed water is increasing, as well as the fact that although the samples were supposed to be "saturated", the pore network was not fully filled with water. After a certain number of cycles, the freeze-thaw damage generates cracking and scaling. Thus the partially filled voids, in conjunction with newly created cracking, provide a transition period. Finally, cracking overcomes the

remaining effects with a significant reduction in UPV (and scaling stands out with a reduction in weight).

As it can be observed from the UPV data in Table 6.3, the UPV values at 23.9 ℃ had to be adjusted to equivalent UPV values at 4.4 ℃, since all UPV measurements of the freeze-thaw samples were collected at 4.4 ℃. But such a relationship as presented in Table 6.2 eventually does not provide an accurate conversion since only three samples were used for the analysis. Furthermore, the microstructure and the saturation level of the pores of samples not exposed to freeze-thaw have been reported to be different than samples that are [55]. Thus the initial UPV values were not used in the modeling that relates UPV and porosity under freeze-thaw conditions in Section 6.7. Besides, the 50, 75, 125, 150 and 175 cycles data were not considered in that analysis either, since measurements of the weight of the samples under water were not available, not allowing the volume/porosity calculations.

6.5 Volume Change during Freeze-Thaw Testing

Sample volume was calculated as the difference in the weights between the SSD sample in air and under water, Equation 6.1, and according to ASTM C642:

$$\boldsymbol{Vol_{solid} = \frac{W_{ssd} - W'}{\rho_w}} \qquad (\mathbf{6.1})$$

where:

Vol_{solid} = volume of solid portion of concrete (i.e. volume of concrete excluding permeable voids), cm^3

W_{ssd} = weight in air of saturated surface dry (SSD) sample, g

W' = weight under water of saturated sample, g

ρ_w = density of water, 1 g/cm^3

Volumes were calculated at 100 cycles, 200 cycles and every 25 cycles afterwards. The results are shown in Table 6.4. An outlier analysis method (as described in section 3.3) was used in these samples' initial volumes.

Table 6.4 Volume with Freeze-Thaw Cycles (cm^3)

Age (days)	29	58	86	93	100	107	116	122	128	135	142
Cycle No. / Sample	0	100	200	225	250	275	300	325	350	375	400
1	1755.6	1755.0	1749.2	--	1749.0	1746.5	1746.9				
2	1760.4	1758.7	1750.3								
3	1747.0	1745.4	1740.6	1741.0	1740.4	1739.4	1738.2	1736.5	1735.7	1734.3	1732.9
4	1739.7	1738.2									
5	1782.0	1779.7	1775.5	1775.7	1774.6	1771.9	1769.8				
6	1795.0	1792.9	1787.1								
7	1798.7	1799.8									
8	1806.9	1809.9	1806.1	1805.6	1803.9	1801.5	1800.9	1797.3	1796.9	1794.2	--
9	1736.6	1736.0	1729.8	1727.8	1726.6	1724.0	1723.1				
10	1776.4	1780.4									
11	1737.7	1739.8	1737.4								
12	1722.8	1723.5	1718.6	1716.3	1714.4	1711.0	1706.6	1702.9	1701.2	1700.9	1700.3
13	1725.5	1727.6									
14	1773.3	1777.7	1771.0	1769.0	1769.2	1768.2	1766.3				
15	1750.5	1752.9	1749.5								
16	1746.0	1748.3									
17	1735.7	1736.7	1733.4	1732.5	1731.6	1729.8	1729.1	1726.8	1725.4	1722.3	1719.3
Mean	1758.2	1759.0	1754.0	1752.6	1751.2	1749.0	1747.6	1740.9	1739.8	1737.9	1736.4

Generally, the volume declined after 100 cycles. The existence of scatters is minimal compared with the trends of weight and UPV. Since the volume measured is the solid portion of concrete which excludes the permeable voids, while SSD weight and UPV are influenced by the presence of the water in these voids. Thus the volume measurements are better indications of the degradation due to freeze-thaw.

The volume change versus freeze-thaw cycles for Sample 17 and the mean values are plotted in Figure 6.3.

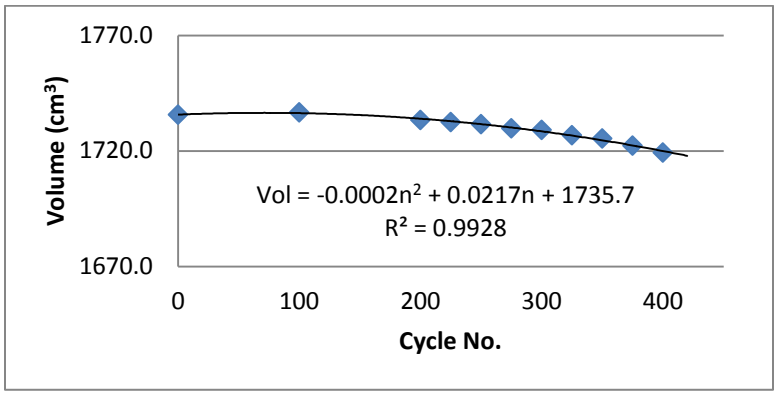

a) Sample 17

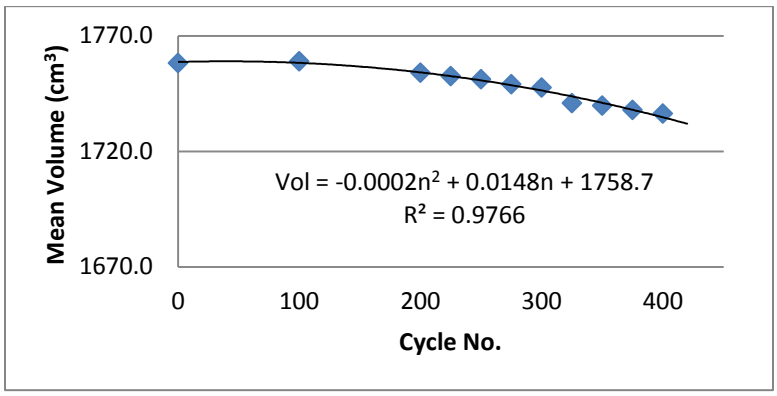

b) Mean Volume of 17 Samples
Figure 6.3 Volume with Freeze-Thaw Cycles

6.6 Porosity Change during Freeze-Thaw Testing

As mentioned previously, water content, density and porosity are important in modeling UPV. Only by monitoring porosity can a mechanism be created to provide insights into UPV with freeze-thaw exposure.

Porosity can be formulated using Equations 4.3 and 6.1.

$$\boldsymbol{p = \frac{W_{ssd} - W_{dry}}{W_{ssd} - W'} * 100\%} \quad (\mathbf{4.3})$$

$$\boldsymbol{Vol_{solid} = \frac{W_{ssd} - W'}{\rho_w}} \quad (\mathbf{6.1})$$

Thus, porosity can be equal to:

$$\boldsymbol{p = \frac{W_{ssd} - W_{dry}}{Vol_{solid}} * 100\%} \quad (\mathbf{6.2})$$

For any sample before freeze-thaw exposure, it can be assumed that:

$$\boldsymbol{W_{dry} = Vol_{solid} * \rho_{solid}} \quad (\mathbf{6.3})$$

where ρ_{solid} is the density of the solid phase of concrete. Thus, by substituting this parameter into Equation 6.3:

$$\boldsymbol{p = \frac{W_{ssd} - Vol_{solid} * \rho_{solid}}{Vol_{solid}} * 100\%} \quad (\mathbf{6.4})$$

Therefore porosity can be obtained as:

$$\boldsymbol{p = (\rho - \rho_{solid}) * 100\%} \quad (\mathbf{6.5})$$

where ρ is the ratio of W_{ssd} and Vol_{solid} (g/cm^3).

Overall, ρ_{solid} is assumed to be constant during freeze-thaw test. Hence p is only affected to the parameter ρ. Once ρ can be determined from experiments, the porosity during freeze-thaw test can be calculated.

It was postulated in Chapter 4 that UPV of control samples are determined by the phase fractions of solid, water and air. Thus it might be possible to relate porosity to freeze-thaw results if it is possible to estimate the porosity of concrete before freeze-thaw exposure.

Using Sample 1 as an example and based on Equation 4.13, which assumes UPV is linear to the total and saturated portions of porosity, the initial porosity can be calculated as:

$$p = p_w = \frac{(4293.14 + 20094.6 - 4.6688 * 5585.4)}{(2.5444 * 1485.7 - 4.6688 * 5585.4)} * 100\% \ = \ 7.577\%$$

Uisng this value into Equation 6.5, the initial concrete density of solid is estimated:

$$\rho_{solid} \ = \frac{3975.5}{1755.6} - 7.577\% = 2.189 \ g/cm^3$$

The layer and exponential relations, as described by Equations 4.15 and 4.17 also yielded a value of 2.189 g/cm^3. It was expected that the calculated ρ_{solid} should be very close by using these three models since they were derived from the same set of data and all three provided comparable correlations. The calculated ρ_{solid} for all 17 samples are shown in Table 6.5. An outlier analysis method (as described in section 3.3) was conducted in these data before analysis.

Table 6.5 Calculated Densities of the Solid Portion of Concrete (g/cm^3)

Sample	Parallel	Layer	Exponential
1	2.189	2.189	2.189
2	2.208	2.208	2.209
3	2.218	2.218	2.219
4	2.137	2.136	2.137
5	2.214	2.214	2.214
6	2.160	2.160	2.160
7	2.158	2.157	2.158
8	2.201	2.200	2.201
9	2.201	2.201	2.201
10	2.193	2.193	2.193
11	2.192	2.192	2.192
12	2.187	2.187	2.187
13	2.214	2.214	2.214
14	2.147	2.147	2.147
15	2.169	2.169	2.169
16	2.198	2.198	2.198
17	2.179	2.179	2.179
Mean	2.186	2.186	2.186
COV (%)	1.118	1.124	1.121

It can be seen that the variability among densities of the solid phase of concrete is very low, regardless which model was used, proving that the concrete mix in the samples was relatively consistent. As expected, the three models (parallel, layered and exponential system) produced negligible differences. What is more, with the assumption that ρ_{solid} of each sample remains constant throughout freeze-thaw testing, the changes of p would be equal to the changes of ρ, as shown by Equation 6.5. In other words, the changes of porosity during freeze-thaw testing are independent of the model used for calculating ρ_{solid}. There is hence no need to individually examine the trend of porosity determined from the three models, but only the porosity derived from linear relation may be selected.

The results are shown in Table 6.6. An outlier analysis method (as described in section 3.3) was employed in these data before analysis.

Example trends for two samples, and the trend of the mean values for all samples are plotted in Figure 6.4.

Table 6.6 Porosity with Freeze-Thaw Cycles (%)

Age (days)	29	58	86	93	100	107	116	122	128	135	142
Cycle No. / Sample	0	100	200	225	250	275	300	325	350	375	400
1	7.577	7.751	8.263	--	8.254	8.339	8.275				
2	7.472	7.989	8.384								
3	7.529	7.911	8.275	8.262	8.175	8.290	8.316	8.369	8.394	8.511	8.570
4	7.909	8.348									
5	7.393	7.660	7.977	7.895	7.919	8.070	8.066				
6	7.458	7.892	8.294								
7	8.219	8.438									
8	7.795	7.754	8.067	8.042	8.152	8.228	8.293	8.394	8.317	8.399	--
9	7.430	7.635	8.047	8.189	8.209	8.240	8.347				
10	7.971	7.904									
11	7.759	7.756	7.885								
12	7.693	7.880	8.165	8.312	8.277	8.448	8.530	8.618	8.745	8.674	8.689
13	7.686	7.662									
14	8.037	7.975	8.298	8.415	8.344	8.442	8.529				
15	7.685	7.959	8.299								
16	7.706	7.693									
17	7.534	7.721	8.001	8.009	7.982	8.072	8.135	8.204	8.173	8.348	8.411
Mean	7.697	7.878	8.163	8.160	8.164	8.266	8.311	8.396	8.407	8.483	8.508

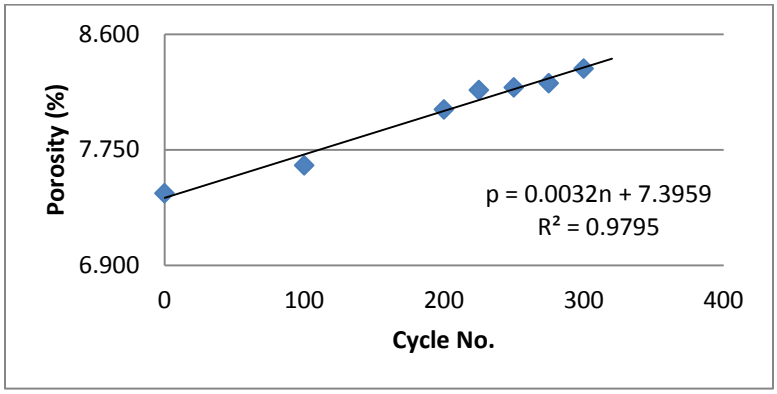

a) Sample 9

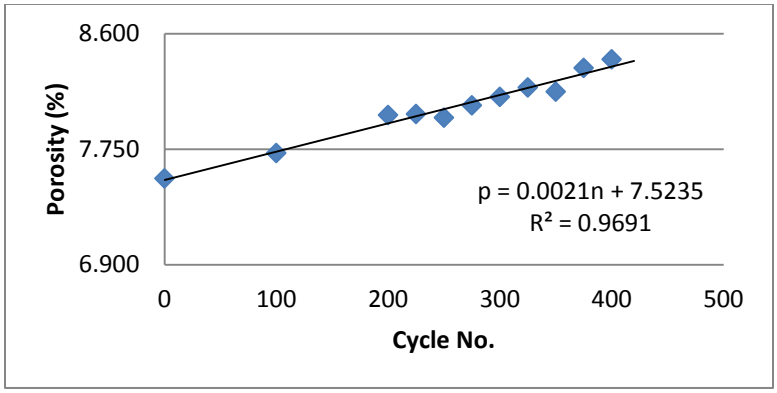

b) Sample 17

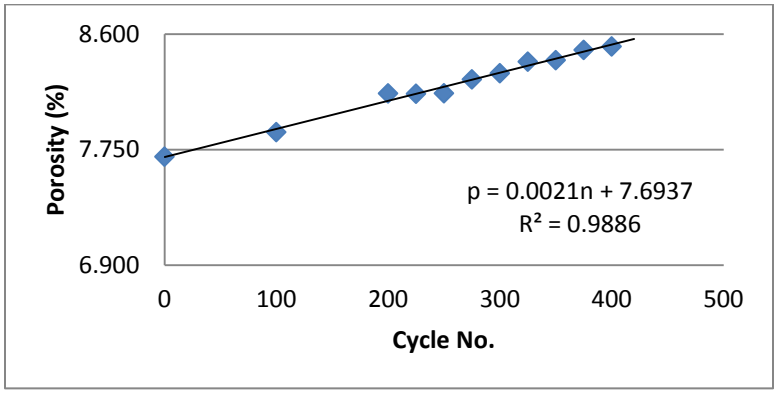

c) Mean Value of 17 Samples

Figure 6.4 Porosity with Freeze-Thaw Cycles

6.7 Freeze-Thaw Modeling

As it was covered in Section 4.5, three models are available to describe the relationship between UPV and porosity.

6.7.1 Parallel System

Equation 4.12b related UPV in a linear relationship to the total and saturated porosity. All pores are assumed to be saturated during the freeze-thaw test (although the trends of weight and UPV have indicated that it might not be true for the initial stages of freeze-thaw), then $p = p_w$. Thus, UPV of the freeze-thaw samples can be modeled with a linear function of porosity, as follows:

$$\boldsymbol{V = c_1 * p + c_2} \qquad (\mathbf{6.6})$$

Considering an example Sample 17, the porosity and corresponding UPV values from 100 cycles are included in Table 6.7.

Table 6.7 Porosity and UPV with Freeze-Thaw Cycles of Sample 17

Cycle No.	p (%)	UPV (m/s)
100	7.721	4431
200	8.001	4387
225	8.009	4348
275	8.072	4315
300	8.135	4294
325	8.204	4228
350	8.173	4296
375	8.348	4135
400	8.411	4172

Regression analysis provided a fairly good relationship between these two parameters, as:

$$\boldsymbol{V(S17) = 7919.95 - 447.15p, with\ R^2 = 0.8939} \qquad (\mathbf{6.7})$$

If porosity changes linearly with freeze-thaw cycles (n), then UPV could be also modeled with a linear function of n, as:

$$\boldsymbol{V = c_3 * n + c_4} \qquad (\mathbf{6.8})$$

Considering again Sample 17 as an example, the regression analysis yielded:

$$\boldsymbol{V(S17) = 4552.97 - 0.930n, with\ R^2 = 0.8388} \qquad (\mathbf{6.9})$$

where *n* is the freeze-thaw cycle count.

If the same regression analysis is conducted on all the samples exposed to 400 cycles, the following regression coefficients, *Ci*, and R^2 are obtained shown in Table 6.8.

Table 6.8 Regression Results for the Parallel Model

	Equation 6.6			Equation 6.8		
Sample	C_1	C_2	R^2	C_3	C_4	R^2
3	-329	7117	0.5520	-0.787	4600	0.8120
8	-411	7823	0.8912	-1.010	4729	0.9064
12	-428	7917	0.9004	-1.198	4650	0.8369
17	-447	7920	0.8939	-0.930	4553	0.8388
COV (%)	-12.87	5.04		-17.47	1.62	

As shown in this table, except Sample 3, all the other samples provided relatively high R^2 using Equation 6.6 and all samples provided relatively high R^2 by using the form of Equation 6.8. Thus the relationship between UPV and freeze-thaw cycle count is as acceptable as the relationship between UPV and porosity.

Clearly, some variability was observed among the four samples, causing variability in the coefficients. Without considering Sample 3, the COV of C_1 and C_3 for the other three samples would be reduced to -4.20 % and -13.15 %, respectively. Thus perhaps Sample 3 had sample-specific preparation or freeze-thaw exposure effects than the rest of the samples.

It was also observed that the intercepts, C_1, are larger than those obtained from the control samples, as shown in Equation 4.13. It is because the pores of the control samples are not as saturated as the samples after freeze-thaw effects. In other words, the control samples "do not" take the pores, which are opened up and filled with water under freeze-thaw testing condition [55], into account, thus resulting in a lower extrapolation of UVP for theoretically zero-porosity concrete.

6.7.2 Layered System

As in Section 4.5, the three phases in concrete, solid, water and air can be modeled using a layered system so that the three fractions are linearly related to the inverse of UPV. Since all pores are assumed to be saturated during the freeze-thaw testing, $p = p_w$. Thus UPV of the freeze-thaw samples can be modeled as:

$$\frac{1}{V} = c_1 * p + c_2 \qquad (6.10)$$

If porosity is linearly related to the freeze-thaw cycle count, n, then UPV could also be modeled with the following function:

$$\frac{1}{V} = c_3 * n + c_4 \qquad (6.11)$$

Applying regression analysis on all 400-cycle-exposure samples, the coefficients and R^2 were obtained shown in Table 6.9.

Table 6.9 Regression Results for the Layered Model

	Equation 6.10			Equation 6.11		
Sample	C_1	C_2	R^2	C_3	C_4	R^2
3	1.704E-03	8.675E-05	0.5497	4.068E-08	2.170E-04	0.8075
8	2.039E-03	5.693E-05	0.8874	5.015E-08	2.110E-04	0.9038
12	2.257E-03	4.147E-05	0.9001	6.330E-08	2.142E-04	0.8389
17	2.434E-03	3.555E-05	0.8857	5.048E-08	2.189E-04	0.8263
COV (%)	14.91	41.50		18.15	1.61	

It can be seen that all samples provided acceptable models using Equation 6.10 except for Sample 3. Also all samples provided acceptable models using Equation 6.11. Thus the relationship between UPV and porosity, and UPV and cycle count are both satisfactory. Compared with the parallel system, this model yielded a slightly lower R^2 for each individual sample.

It is obvious that the four samples have a large variability among the regression coefficients and R^2. If Sample 3 is excluded, the COV of C_1 and C_3 for the other three samples would be reduced to 8.81 % and 13.73 %, respectively. It was thus believed that Sample 3 is very likely to behave or be exposed differently from the rest.

6.7.3 Exponential System

As in Section 4.5, an exponential relationship can be built between UPV and the volume fractions of solid, water and air. Since all pores are assumed to be saturated in the freeze-thaw testing, thus UPV of the freeze-thaw samples can be modeled as follows:

$$\boldsymbol{V = V_{p0}(1-p)^{c_1}} \qquad \boldsymbol{(6.12)}$$

Applying regression analysis on all 400 cycle samples individually, the coefficients and R^2 are shown below.

Table 6.10 Regression Results for the Exponential Model (Equation 6.12)

Sample	V_{p0}	C_1	R^2
3	7941	6.881	0.5512
8	9145	8.414	0.8895
12	9513	9.010	0.9005
17	9638	9.593	0.8904
COV (%)	8.55	13.76	

Again, all samples provided acceptable models using Equation 6.12 except Sample 3. Compared with the above two models, this model yielded similar R^2 for each individual sample.

Although a non-neglectable variability among the regression coefficients and R^2 was observed, it is smaller compared to the previous two models. If Sample 3 is excluded, COV of V_{p0} and C_1 for the other three samples would be reduced to 2.71 % and 4.54 %, respectively. Thus this model might be better at averaging the samples variations.

6.7.4 Relationship between Ultrasonic Pulse Velocity and changes of Porosity

Even though the three models discussed above provided good results based on the data of the individual samples, the variability among samples needs to be considered. In order to avoid the difference in samples' properties and exposure, the changes of UPV and porosity since 100 freeze-thaw cycles should be employed, as shown in Figure 6.5. As a result, instead of using the actual values of V and p, the changes, ΔV and Δp, from 100 to 400 cycles were calculated and related, as presented in Table 6.10 and Figure 6.6, while the regression model is provided in Equation 6.13.

Table 6.11 Changes of porosity and UPV from 100 to 400 Freeze-Thaw Cycles

Sample	Cycle No.	Δp (%)	ΔV (m/s)
3	100	0.000	0
	200	0.364	-12
	225	0.351	-59
	250	0.264	-109
	275	0.379	-74
	300	0.405	-187
	325	0.458	-124
	350	0.483	-181
	375	0.600	-195
8	100	0.000	0
	200	0.313	-65
	225	0.288	-138
	250	0.397	-146
	275	0.474	-186
	300	0.539	-258
	325	0.640	-226
	350	0.563	-216
	375	0.645	-270
12	100	0.000	0
	200	0.285	-15
	225	0.432	-197
	250	0.398	-156
	275	0.568	-197
	300	0.650	-239
	325	0.739	-328
	375	0.794	-286
	400	0.810	-325
17	100	0.000	0
	200	0.279	-44
	225	0.287	-83
	275	0.351	-116
	300	0.413	-137
	325	0.483	-202
	350	0.452	-134
	375	0.626	-295
	400	0.689	-258

Note: Number of repeated UPV measurements = 5

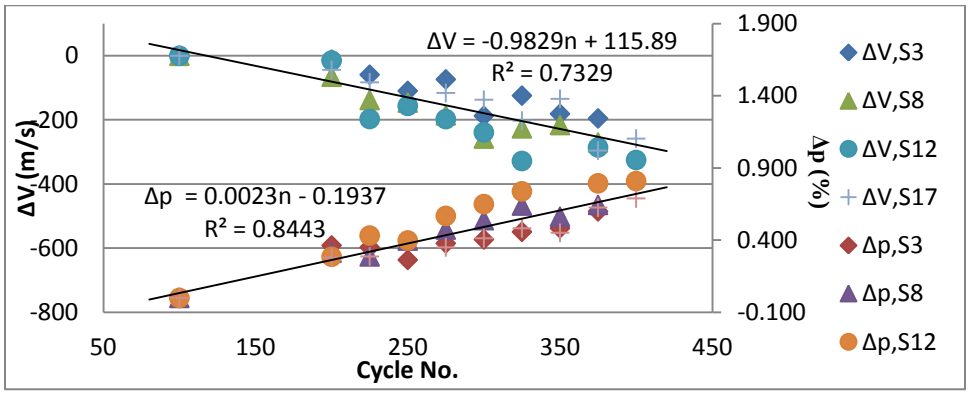

Figure 6.5 ΔV and Δp with Freeze-Thaw Cycles

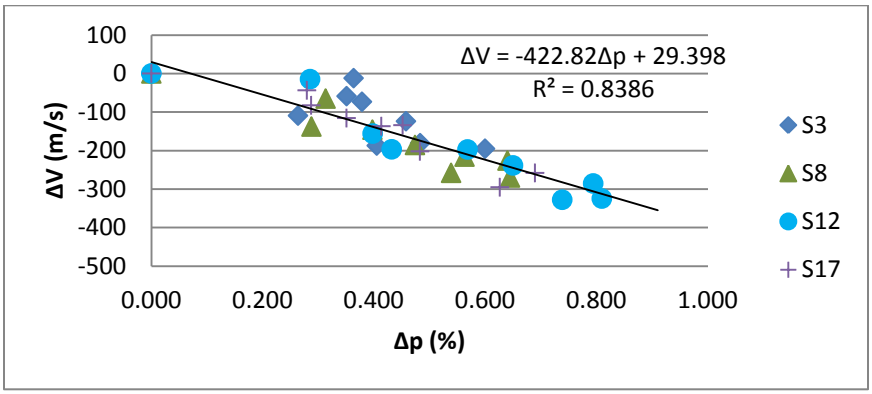

Figure 6.6 Relationship between ΔV and Δp

$$\boldsymbol{\Delta V = -422.82\Delta p + 29.40, with\ R^2 = 0.8386} \qquad \textbf{(6.13)}$$

where ΔV is the change of UPV from 100 cycles (m/s) and Δp is the change of porosity (%) from 100 cycles. Such a relationship is quite satisfactory (R^2= 0.8386).

6.8 Discussion and Conclusion

In this chapter, modeling was conducted to develop the relationship between UPV and concrete properties under freeze-thaw effects. Weight and volume values were used in this analysis. The data indicated that the SSD weight increased to about 100 cycles, and decreased after that. The volume had a continuous declining trend after 100 cycles. UPV reached and stayed at the peak between 100 to 200 cycles, and then decreased as the number of freeze-thaw cycles increased.

Concrete porosity was used to relate UPV values with the weight and volume measurements. Based on the relationship described in Equation 6.5, porosity can be determined from concrete density. Once ρ can be obtained from experimental data, porosity changes with freeze-thaw cycles can be calculated. The analysis showed that porosity increases linearly with freeze-thaw cycles.

The relationships between UPV and porosity for freeze-thaw samples were developed with three models, the parallel, the layered and the exponential system. It was found that all three models provide acceptable results when using freeze-thaw data from individual samples. In order to develop a relationship that considers all samples together, the change in UPV and porosity, with the data from all samples starting from 100 freeze-thaw cycles on, were used instead of the actual values. The results generated are satisfactory and sample-independent.

7 Conclusions and Recommendations

7.1 Conclusions

The primary objective of this investigation was to determine the effectiveness of using ultrasonic pulse velocity (UPV) to detect damage in fiber reinforced concrete (FRC) under fatigue and freezing-thawing conditions. In order to achieve this, testing on control samples was conducted to quantify the effects of water content, porosity, density on UPV. Furthermore, samples exposed to both fatigue and freeze-thaw testing were used as well for evaluating the ability of UPV to detect concrete damage.

The specific conclusions include:

1) UPV in concrete depends on a variety of concrete properties and environmental conditions. Relationships between UPV and water content, concrete age, concrete density, compressive strength and flexural were examined.
2) The relationship between UPV and porosity was established using UPV measurement on SSD and dry samples.
3) Three models, the parallel system, the layered system and the exponential system can be used for modeling UPV with total porosity, water-filled porosity, and free porosity. Each of those models provided comparable results.
4) UPV is promising in detecting artificial cut beyond a certain size. The "full contact" was found to have the benefits of ease to set up and high correlation with cut depth.

5) Unless a more thorough understanding of the fatigue failure mechanism in concrete is available, UPV has limited use for detecting damage under fatigue.
6) Porosity of saturated concrete was related to concrete density and thus can be assessed with a simple laboratory procedure. Porosity was found to increase linearly with freeze-thaw cycles.
7) Relationships between UPV and porosity under freeze-thaw conditions were developed. The three models used for the control samples (parallel, layered and exponential system) can also be applied for freeze-thaw samples with satisfactory results.
8) The changes of UPV and porosity were related. Consequently, once the change of UPV at a certain freeze-thaw cycle is measured, the relative porosity/damage can be determined, and vice versa.

7.2 Recommendations

The following recommendations are intended for future research in this area to further examine the applicability of UPV in detecting damage:

1) Since UPV is influenced by a manifold of concrete properties such as age, water content, temperature, wave frequency etc, a systematic study is needed to properly identify correction to UPV values based on these parameters for a specific concrete mix.
2) The UPV-porosity models developed in this research should be further expanded by including additional mixtures into the analysis. The porosity

determined from the permeable voids should be compared to more accurate measurement of porosity. The classifications of pores based on the size and shape as well as the filled water, which might be distinctive from free water, will provide more insights into the models. Such work will extend the validity and improve the response of the models.

3) Because of the high variability in fatigue lives, there is a need to thoroughly understand and model the fatigue failure mechanism. With such, it will be possible to predict the final stage of fatigue, thus to carry out UPV testing at proper intervals. Also, in-situ UPV testing should be developed to avoid moving a significantly damaged sample from the fatigue pedestal.
4) Further exposure to freeze-thaw cycles should be considered for further validating the results of this study. Although periodic monitoring of the samples can provide details on concrete damage, it is more critical to monitor the damage stages close to failure. The variability of the freeze-thaw effects in various locations needs to be averaged with a larger sample population.
5) The models accounting for the porosity of concrete samples can be further improved by considering the portion of the "neglected" pores, which are opened up under freeze/thaw, in the control samples. The process of water penetrating into the pores in the initial stages of freeze-thaw should also be accounted. In such a case improved models can be developed that connect control samples and samples exposed to freezing and thawing.

6) Finally, the UPV modeling presented in this research needs to be developed and calibrated for field conditions.

Appendix

The results from the UPV and fatigue analysis for Samples 1, 2 and 3 are presented in Tables A.1 through A.3.

Table A. 1 UPV and Fatigue Cycles of Sample 1 (s/Mr=0.75, 5 Hz)

Cycle No.	Corner	Transit Time (μs)					Mean (μs)	UPV (m/s)	Average UPV (m/s)	% Change
5000	1	66.0	65.9	66.2	66.2	66.0	66.1	4616	4591	--
	4	66.9	66.8	66.7	67.0	66.5	66.8	4566		
7000	1	66.6	66.6	67.5	67.4	67.2	67.1	4547	4495	-2.08
	4	68.7	68.9	69.0	68.4	68.1	68.6	4443		
9000	1	66.5	69.1	67.8	67.4	65.9	67.3	4528	4527	0.71
	4	68.0	67.6	67.3	66.8	67.1	67.4	4526		
11000	1	66.6	66.6	65.8	65.9	66.4	66.3	4602	4522	-0.12
	4	68.2	69.2	68.5	68.6	68.7	68.6	4442		
13000	1	68.0	67.7	67.7	66.8	66.2	67.3	4532	4506	-0.35
	4	67.8	68.4	68.1	67.9	68.1	68.1	4480		
15000	1	69.1	68.1	68.0	68.6	67.9	68.3	4462	4481	-0.56
	4	68.0	68.0	67.8	67.4	67.6	67.8	4500		
17000	1	68.1	68.6	67.6	66.9	66.9	67.6	4509	4525	0.99
	4	67.3	67.1	67.0	67.1	67.2	67.1	4541		
19000	1	65.1	66.2	66.1	65.8	66.1	65.9	4630	4547	0.48
	4	68.7	68.2	67.9	68.2	68.5	68.3	4464		
23000	1	65.2	65.4	65.3	65.4	65.7	65.4	4662	4594	1.03
	4	67.4	67.9	67.1	67.5	67.0	67.4	4525		
27000	1	65.2	65.4	65.3	65.4	65.7	65.4	4662	4594	0.00
	4	67.4	67.9	67.1	67.5	67.0	67.4	4525		
29100	Failure									

Note: Corner 1 and Corner 4 are bottom and top during casting, respectively

Table A. 2 UPV and Fatigue Cycles of Sample 2 (s/Mr=0.75, 5 Hz)

Cycle No.	Corner	Transit Time (μs)					Mean (μs)	UPV (m/s)	Average UPV (m/s)	% Change
19000	1	65.6	65.5	65.6	65.6	65.4	65.5	4654	4609	--
	4	66.3	67.0	66.9	67.0	66.9	66.8	4564		
23000	1	64.6	65.3	65.3	65.4	65.3	65.2	4679	4628	0.41
	4	66.4	66.7	66.9	66.9	66.3	66.6	4576		
27000	1	65.8	65.5	65.5	65.2	65.9	65.6	4651	4581	-1.02
	4	67.7	67.5	67.5	67.8	67.6	67.6	4510		
28000	1	65.2	65.4	66.1	65.0	65.6	65.5	4659	4599	0.40
	4	67.4	67.0	67.3	67.1	67.2	67.2	4538		
28500	1	65.0	65.2	66.0	66.0	65.6	65.6	4652	4600	0.03
	4	66.8	67.2	66,6	67.1	67.1	67.1	4549		
29000	1	65.0	65.4	65.4	68.0	67.7	66.3	4600	4575	-0.54
	4	67.1	66.7	66.7	67.1	67.5	67.0	4551		
29500	1	67.6	68.2	65.8	65.5	65.8	66.6	4581	4566	-0.20
	4	67.1	66.7	66.8	67.0	67.4	67.0	4552		
30000	1	65.2	65.7	65.6	65.7	65.6	65.6	4652	4601	0.75
	4	66.7	67.4	67.2	66.9	67.0	67.0	4549		
31000	1	65.9	65.6	65.7	65.2	65.0	65.5	4658	4618	0.37
	4	66.7	66.2	66.4	66.8	67.0	66.6	4578		
32000	1	64.8	65.4	65.6	65.6	65.1	65.3	4671	4615	-0.05
	4	67.4	66.6	66.7	67.1	66.6	66.9	4560		
34000	1	65.6	65.7	65.2	64.8	65.3	65.3	4669	4603	-0.27
	4	67.8	66.9	66.9	67.1	67.4	67.2	4537		
41260	Failure									

Note: Corner 1 and Corner 4 are bottom and top during casting, respectively

Table A. 3 UPV and Fatigue Cycles of Sample 3 (s/Mr=0.75, 5 Hz)

Cycle No.	Corner	Transit Time (μs)					Mean (μs)	UPV (m/s)	Average UPV (m/s)	% Change
20000	1	65.7	65.9	66.2	66.6	66.8	66.2	4654	4609	--
	4	68.1	68.6	68.2	68.4	68.6	68.4	4564		
22000	1	66.7	66.8	66.8	65.8	66.2	66.5	4679	4628	0.41
	4	67.5	67.8	67.8	67.4	67.7	67.6	4576		
23000	1	65.5	65.8	65.4	65.3	65.7	65.5	4651	4581	-1.02
	4	67.6	67.8	67.8	67.4	67.4	67.6	4510		
24000	1	65.5	64.7	65.2	65.0	64.7	65.0	4659	4599	0.40
	4	67.2	67.0	66.5	66.7	66.7	66.8	4538		
25000	1	64.4	64.5	64.2	64.0	65.1	64.4	4652	4600	0.03
	4	66.5	66.6	66.6	66.5	67.0	66.6	4549		
26000	1	65.9	64.4	65.1	64.8	64.8	65.0	4600	4575	-0.54
	4	67.4	67.2	67.0	67.2	67.1	67.2	4551		
27000	1	64.9	65.0	65.7	65.6	65.4	65.3	4581	4566	-0.20
	4	66.9	68.0	68.0	67.8	67.3	67.6	4552		
28000	1	64.6	65.5	65.3	64.7	65.4	65.1	4652	4601	0.75
	4	67.9	67.5	67.4	67.7	68.0	67.7	4549		
29000	1	65.5	65.7	65.5	65.6	65.2	65.5	4658	4618	0.37
	4	67.3	67.0	67.5	67.3	67.8	67.4	4578		
30000	1	65.5	65.9	65.3	66.0	65.2	65.6	4671	4615	-0.05
	4	68.1	68.9	68.1	67.6	68.1	68.2	4560		
30500	1	65.0	65.9	65.5	66.2	66.2	65.8	4669	4603	-0.27
	4	68.0	68.5	68.6	69.0	68.0	68.4	4537		
30700	Failure									

Note: Corner 1 and Corner 4 are bottom and top during casting, respectively

Literature

1. Lee, M. and B. Barr, *An Overview of the Fatigue Behaviour of Plain and Fibre Reinforced Concrete.* Cement and Concrete Composites, 2004. **26**(4): p. 299-305.
2. Richardson, A., *Freeze/Thaw Durability in Concrete with Fibre Additions.* Structural Survey, 2003. **21(5)**.
3. Popovics, J.S. and J.L. Rose, *A Survey of Developments in Ultrasonic NDE of Concrete.* Ultrasonics, Ferroelectrics and Frequency Control, IEEE Transactions on, 1994. **41**(1): p. 140-143.
4. Kočiš, Š. and Z. Figura, *Ultrasonic Measurements and Technologies*. Vol. 4. 1996: Chapman & Hall.
5. Richardson, M., *Fundamentals of Durable Reinforced Concrete*2002: Taylor & Francis.
6. Ozyildirim, C., C. Moen, and S. Hladky, *Investigation of Fiber-Reinforced Concrete for Use in Transportation Structures.* Transportation Research Record: Journal of the Transportation Research Board, 1997. **1574**(-1): p. 63-70.
7. Nagabhushanam, M., V. Ramakrishnan, and G. Vondran, *Fatigue Strength of Fibrillated Polypropylene Fiber Reinforced Concretes.* Transportation Research Record, 1989(1226).
8. Vondran, G., M. Nagabhushanam, and V. Ramakrishnan, *Fatigue strength of polypropylene fiber reinforced concretes.* Elsevier Applied Science, 1989: p. 533-543.
9. Zia, P., M.L. Leming, and S.H. Ahmad, *High-performance concretes: A state-of-the-art report*, 1991, North Carolina State Univ., Raleigh, NC (United States).
10. Bayasi, Z. and J. Zeng, *Properties of Polypropylene Fiber Reinforced Concrete.* ACI Materials Journal, 1993. **90**(6).
11. R-96, A., *State-of-the-Art Report on Fiber Reinforced Concrete*, 1997, American Concrete Institute.
12. Janssen, D.J. and M.B. Snyder, *Resistance of Concrete to Freezing and Thawing*1994.
13. Neville, A.M., *Properties of Concrete*1995.
14. Powers, T., *Freezing Effects in Concrete.* Durability of concrete, 1975: p. 1-11.
15. Lamond, J.F., *Significance of Tests and Properties of Concrete and Concrete-Making Materials*. Vol. 169. 2006: Astm International.
16. Bayasi, Z. and T. Celik, *Application of Silica Fume in Synthetic Fiber-Reinforced Concrete.* Transportation Research Record, 1993(1382).
17. Al-Tayyib, A.H.J. and M.M. Al-Zahrani, *Use of Polypropylene Fibers to Enhance Deterioration Resistance of Concrete Surface Skin Subjected to Cyclic Wet/Dry Seawater Exposure.* ACI Materials Journal, 1990. **87**(4).
18. Bungey, J.H., S.G. Millard, and M. Grantham, *Testing of Concrete in Structures*2006: Routledge.
19. Malhotra, V.M. and N.J. Carino, *Handbook on Nondestructive Testing of Concrete*2004: ASTM International.
20. Ye, G., K. Van Breugel, and A. Fraaij, *Experimental study on ultrasonic pulse velocity evaluation of the microstructure of cementitious material at early age.* Heron, 2001. **46**(3): p. 161-167.
21. Trtnik, G., F. Kavcic, and G. Turk, *Prediction of concrete strength using ultrasonic pulse velocity and artificial neural networks.* Ultrasonics, 2009. **49**(1): p. 53-60.

22. Madandoust, R., R. Ghavidel, and N. Nariman-Zadeh, *Evolutionary Design of Generalized GMDH-Type Neural Network for Prediction of Concrete Compressive Strength Using UPV.* Computational Materials Science, 2010. **49**(3): p. 556-567.
23. Ohdaira, E. and N. Masuzawa, *Water Content and Its Effect on Ultrasound Propagation in Concrete—the Possibility of NDE.* Ultrasonics, 2000. **38**(1): p. 546-552.
24. Yaman, I., N. Hearn, and H. Aktan, *Active and non-active porosity in concrete part I: experimental evidence.* Materials and Structures, 2002. **35**(2): p. 102-109.
25. Popovics, S., *Effects of Uneven Moisture Distribution on the Strength of and Wave Velocity in Concrete.* Ultrasonics, 2005. **43**(6): p. 429-434.
26. Popovics, S., *Analysis of the Concrete Strength Versus Ultrasonic Pulse Velocity Relationship.* American Society for Nondestructive Testing, 2007.
27. Lin, Y., C.P. Lai, and T. Yen, *Prediction of Ultrasonic Pulse Velocity (UPV) in Concrete.* ACI Materials Journal, 2003. **100**(1).
28. Peterson, K.W., *Automated Air-void System Characterization of Hardened Concrete: Helping Computers to Count Air-voids Like People Count Air-voids -- Methods for Flatbed Scanner Calibration*2008: Michigan Technological University.
29. Yaman, I., O. Udegbunam, and H. Aktan, *Assessing concrete permeability from ultrasonic pulse velocity measurements.* Transportation Research Board, 2000.
30. Komlos, K., et al., *Ultrasonic Pulse Velocity Test of Concrete Properties as Specified in Various Standards.* Cement and Concrete Composites, 1996. **18**(5): p. 357-364.
31. Reinhardt, H., C. Grosse, and A. Herb, *Ultrasonic Monitoring of Setting and Hardening of Cement Mortar—A New Device.* Materials and Structures, 2000. **33**(9): p. 581-583.
32. Zhang, Y., et al., *Ultrasound monitoring of setting and hardening process of ultra-high performance cementitious materials.* NDT & E International, 2009.
33. Khan, M.I., *Evaluation of Non-Destructive Testing of High Strength Concrete Incorporating Supplementary Cementitious Composites.* Resources, Conservation and Recycling, 2012. **61**: p. 125-129.
34. Popovics, S., J.L. Rose, and J.S. Popovics, *The Behaviour of Ultrasonic Pulses in Concrete.* Cement and Concrete Research, 1990. **20**(2): p. 259-270.
35. Panzera, T.H., et al., *Correlation between Structure and Pulse Velocity of Cementitious Composites.* Advances in cement research., 2008. **20**(3): p. 101-108.
36. Turgut, P., *Evaluation of the Ultrasonic Pulse Velocity Data coming on the Field.* IBIS, 2004. **6**: p. 8.
37. Nash't, I.H., S.H. A'bour, and A.A. Sadoon. *Finding an Unified Relationship between Crushing Strength of Concrete and Non-Destructive Tests*. in *Middle East Nondestructive Testing Conference & Exhibition, Bahrain*. 2005. Citeseer.
38. Kheder, G., *A Two Stage Procedure for Assessment of In-Situ Concrete Strength Using Combined Non-Destructive Testing.* Materials and Structures, 1999. **32**(6): p. 410-417.
39. Del Rıo, L., et al., *Characterization and Hardening of Concrete with Ultrasonic Testing.* Ultrasonics, 2004. **42**(1): p. 527-530.
40. Shariati, M., et al., *Assessing the strength of reinforced concrete structures through Ultrasonic Pulse Velocity and Schmidt Rebound Hammer tests.* Scientific Research and Essays, 2011. **6**(1): p. 213-220.
41. Van Hauwaert, A., J.F. Thimus, and F. Delannay, *Use of ultrasonics to follow crack growth.* Ultrasonics, 1998. **36**(1): p. 209-217.
42. Nixon, P., *Recycled Concrete as an Aggregate for Concrete—A Review.* Materials and Structures, 1978. **11**(5): p. 371-378.

43. Richardson, A., et al., *Freeze/Thaw Performance of Concrete Using Granulated Rubber Crumb.* Journal of Green Building, 2011. **6**(1): p. 83-92.
44. Kelly, B. and P. Murphy, *Prediction of Freeze-thaw Resistance of Concrete*, in *SCHOOL OF ARCHITECTURE, LANDSCAPE AND CIVIL ENGINEERING*2010, UNIVERSITY COLLEGE DUBLIN.
45. Şahmaran, M., M. Lachemi, and V.C. Li, *Assessing the Durability of Engineered Cementitious Composites under Freezing and Thawing Cycles.* JOURNAL OF ASTM INTERNATIONAL, 2009.
46. Romero, H.L., M.J. Casati, and J.C. Gálvez, *NDT for Concrete under Accelerated Freeze/Thaw Tests and Surface Scaling.* Concrete Technology, 2011.
47. Erdélyi, A., et al., *Deterioration of Steel Fibre Reinforced Concrete by Freeze-Thaw and De-Icing Salts.* CONCRETE STRUCTURES, 2008.
48. Selleck, S.F., et al., *Ultrasonic Investigation of Concrete with Distributed Damage.* Aci Materials Journal, 1998. **95**(1): p. 27-36.
49. Fadragas, C.R. and M.R. González, *Dependence of Ultrasonic Pulse Propagation Velocity on Free Water Content in Concrete Structure under Tropical Climate Conditions.* 2010.
50. Jones, R. *Testing of Concrete by Ultrasonic-Pulse Technique*. 1953.
51. Kaplan, M., *The Effects of Age and Water/Cement Ratio Upon The Relation Between Ultrasonic Pulse Velocity and Compressive Strength.* Mag Con Res, 1959. **11**(32): p. 85-92.
52. Anderson, D.A. and R.K. Seals. *Pulse Velocity as a Predictor of 28-and 90-Day Strength*. 1981. ACI.
53. Jones, R., *Non-Destructive Testing of Concrete*1962: University Press.
54. Fagerlund, G., *On the Service Life of Concrete Exposed to Frost Action*1997.
55. Fagerlund, G., *The critical degree of saturation method of assessing the freeze/thaw resistance of concrete.* Materials and Structures, 1977. **10**(4): p. 217-229.